Updated cosmic-ray and radio constraints on light dark matter: Implications for the GeV gamma-ray excess at the Galactic Center

Torsten Bringmann,[1,*] Martin Vollmann,[2,†] and Christoph Weniger[3,‡]

[1]*Department of Physics, University of Oslo, Box 1048, NO-0316 Oslo, Norway*
[2]*II. Institute for Theoretical Physics, University of Hamburg, Luruper Chaussee 149, 22761 Hamburg, Germany*
[3]*GRAPPA, University of Amsterdam, Science Park 904, 1090 GL Amsterdam, Netherlands*

(Received 1 September 2014; published 1 December 2014)

The apparent gamma-ray excess in the Galactic center region and inner Galaxy has attracted considerable interest, notably because both its spectrum and its radial distribution are consistent with an interpretation in terms of annihilating dark matter particles with a mass of about 10–40 GeV. We confront such an interpretation with an updated compilation of various indirect dark matter detection bounds, which we adapt to the specific form required by the observed signal. We find that cosmic-ray positron data strongly rule out dark matter annihilating to light leptons, or "democratically" to all leptons, as an explanation of the signal. Cosmic-ray antiprotons, for which we present independent and significantly improved limits with respect to previous estimates, are already in considerable tension with dark matter (DM) annihilation to any combination of quark final states; the first set of AMS-02 data will thus be able to rule out or confirm the DM hypothesis with high confidence. For reasonable assumptions about the magnetic field in the Galactic center region, radio observations independently put very severe constraints on a DM interpretation of the excess, in particular for all leptonic annihilation channels.

DOI: 10.1103/PhysRevD.90.123001 PACS numbers: 98.70.Rz, 95.35.+d, 98.70.Sa

I. INTRODUCTION

Because of the high expected dark matter (DM) density, the inner part of the Galaxy is one of the prime targets for indirect searches for particle DM (for recent reviews, see Refs. [1–3]). Indeed, indications for DM signals from the Galactic center (GC) region have repeatedly appeared in the past—in particular in gamma rays [4–10], but also in microwaves [11] and the annihilation radiation from positrons [12]. This part of the Galaxy, however, is also an astrophysically very rich environment. Unless one can identify a distinct spectral signature [13,14], this generally makes disentangling any potential DM signal from astrophysical backgrounds a formidable task. In fact, more refined analyses and new data have so far always tended to disfavor the DM hypotheses previously put forward [15–19]. The field has matured significantly in recent years, however, concerning both the understanding of astrophysical backgrounds and the statistical analysis of potential signals, not the least because of the unprecedented wealth of high-quality data that now are at our disposal. At the same time, many theoretical models predict signals just below current exclusion limits. This implies both that more signal claims should be expected in the near future and that those should not be dismissed too easily.

An example for such a sophisticated analysis is the recent discussion of the GeV gamma-ray excess in Fermi-LAT [20] data of the GC and inner Galaxy [21], which reconfirms corresponding earlier findings [22–29] with a high level of detail (see also Ref. [30] for a review). The spectrum of the excess seen at the GC can be well described by the annihilation of 10–40 GeV DM particles into quarks, or leptons, which then produce secondary photons during their fragmentation and decay. Indeed, the signal normalization is consistent with that expected for thermally produced DM. The observed spectrum, however, does not contain the type of sharp features that would unambiguously point to a DM origin. It is thus arguably even more interesting that the signal is spherically symmetric and that it is claimed to extend to at least 1.5 kpc away from the GC [28], where astrophysical backgrounds with a similar morphology are expected to be strongly suppressed. Last but not least, the excess emission decreases with galactocentric distance in a way that is consistent with the wide range of expectations for annihilating DM. Not surprisingly, the most recent analysis of this excess [21] has already triggered a considerable activity in concrete model-building attempts [31–42].

If the excess can indeed be attributed to annihilating DM particles, this will also leave traces in other cosmic-ray fluxes. In fact, a confirmation of the DM hypothesis essentially *requires* one to find corroborating evidence from a different type of experiment, and observations using other cosmic-ray messengers or photons at other wavelengths seem to be a particularly natural choice to look for

*Torsten.Bringmann@fys.uio.no
†Martin.Vollmann@desy.de
‡C.Weniger@uva.nl

such a second signal (while the translation to expected rates in direct detection experiments or at colliders is much more model dependent). Given the renewed interest in the GC gamma-ray excess, we thus present here an updated collection of constraints deriving from indirect DM searches. In particular, we point out that the observed radial distribution of the gamma-ray signal essentially fixes the DM distribution in the inner Galaxy, thereby significantly reducing the astrophysical uncertainties typically associated with such limits. This allows one to reliably constrain the DM interpretation of the signal, almost independent of the DM profile and much less model dependent than corresponding constraints derived from DM searches at colliders or in direct detection experiments [43–47].

This article is organized as follows. We start in Sec. II by reviewing the current situation of the GeV excess, with an emphasis on the possibility that it is induced by annihilating DM. In Sec. III we present updated bounds on this interpretation from other indirect searches for DM, in particular using cosmic-ray antiprotons and positrons, as well as radio observations. We provide a more detailed discussion of systematic uncertainties for the most relevant limits in Sec. IV and a summary in terms of the main possible DM annihilation channels in context of the GC GeV excess in Sec. V. In Sec. VI, finally, we conclude.

II. CHARACTERISTICS OF THE GEV EXCESS

The DM interpretation of the excess emission at the GC is suggestive in a number of ways: The extended emission appears to peak relatively sharply at energies around 1–3 GeV, is rotationally symmetric around the GC, and roughly follows a $\propto r^{-2.5}$ emission profile, compatible with the annihilation signal from a standard cuspy—if slightly contracted—DM distribution [23]. Furthermore, the same spectral signature was claimed to extend to much higher Galactic latitudes, $|b| \gtrsim 10^\circ$ [28] (see also Ref. [29]). Indeed, a signal from DM annihilation is in general expected to extend to high latitudes, and it can even be visible at the Galactic poles if the substructure enhancement of the annihilation signal is significant at cosmological distances. Astrophysical explanations in terms of millisecond pulsars (MSPs), bremsstrahlung, or neutral pion decay close to the GC are not yet excluded, but would all face serious challenges if—despite the sizable systematic uncertainties [48]—the extension of the GeV excess to Galactic latitudes of $|b| > \mathcal{O}(10^\circ)$ is confirmed. It should in fact be stressed that the nominal statistical significance of the excess is extremely high (e.g., at the level of $\sim 40\sigma$ in the inner Galaxy analysis of Ref. [21]), and that by now background modeling uncertainties are the main limiting factor in characterizing its properties.

First claims that the gamma-ray emission from the GC as seen by Fermi-LAT suggests a DM annihilation signal were put forward in Ref. [22], using a simple power-law model for the spectrum of Galactic diffuse emission. The authors found that annihilation into $\bar{b}b$ final states, a DM mass around 25–30 GeV, and an annihilation cross section close to the thermal value are compatible with the data. In Ref. [23] the same authors found that the dominant part of the emission comes from the inner 1.25° around the GC, with a volume emissivity that scales like $\sim r^{-2.5}$, and discussed possible astrophysical interpretations in terms of MSPs (first mentioned in Ref. [49]; see also Ref. [50] for a much earlier discussion in the context of EGRET measurements) and neutral pion decay from cosmic-ray interactions. Reference [24] presented an updated analysis, using three years of Pass 7 Fermi-LAT data, and arriving at similar conclusions. Reference [51] pointed out the importance of a proper treatment of point sources close to the GC.

In an independent analysis, Ref. [25] confirmed the existence of a significant extended emission at the GC and found it well compatible with the spectrum of known MSPs. Alternative scenarios discussed in the literature are bremsstrahlung of electrons on molecular gas [52] within the inner few hundred pc, or proton-proton interaction within the inner few pc of the supermassive black hole (SMBH) [53]. In Ref. [54], the authors study some of the systematic uncertainties related to standard emission models for the diffuse backgrounds at the Galactic center and find that—after marginalizing over point sources and diffuse background uncertainties—both DM annihilation and a population of at least ~1000–2000 MSPs are compatible with the excess emission from the Galactic center.

The latest analyses of the GC excess emission were presented in Ref. [27], discussing in some detail background modeling systematics related to point sources, molecular gas, and generic extended diffuse emission, and in Ref. [21], which updates previous analyses by using a subset of Fermi-LAT data with improved angular resolution (based on a cut on CTBCORE [55]). For definiteness, we will mostly base the discussion in this paper on the results obtained in Ref. [21].

A. DM interpretation

Focusing on the DM interpretation of the GeV excess, let us first have a detailed look at what the observations would tell us about the annihilating particles. For definiteness, we will do this for a number of benchmark scenarios—based on the results from Ref. [21], but additionally including uncertainties related to the DM distribution.

The differential intensity of photons from DM annihilation as observed at Earth can be calculated via

$$\frac{d\phi}{dEd\Omega} = \frac{1}{4\pi}\int_{\text{l.o.s.}} ds \underbrace{\frac{\langle\sigma v\rangle}{2m_\chi^2}\frac{dN_\gamma}{dE}}_{\equiv Q(r,E)}\rho(r)^2, \qquad (1)$$

where $\langle\sigma v\rangle$ is the average velocity-weighted annihilation cross section, m_χ denotes the DM mass, dN_γ/dE is the energy spectrum of prompt photons produced in the annihilation, and $\rho(r)$ is the DM density as a function of the galactocentric radius r. The integral runs over the line-of-sight parameter s, and r is given by $r = \sqrt{(R_\odot - s\cos\psi)^2 + (s\sin\psi)^2}$, where $R_\odot = 8.5$ kpc is the distance between the Sun and GC, and ψ is the angle to the GC. Last, we defined $Q(r, E)$ as the *differential injection rate* of gamma rays from DM annihilation.

When extrapolating the excess emission observed at the GC to other points in the Galaxy, the main unknown is the shape of the Galactic DM halo and the distribution of DM substructures. The infall of baryons onto the central regions during galaxy formation can cause adiabatic contraction of the DM halo [56]. The exact strength of this effect is unknown, and we will here use a generalized Navarro-Frenk-White (NFW) profile [57], given by

$$\rho(r) = \rho_\odot \left(\frac{r}{R_\odot}\right)^{-\Gamma} \left(\frac{r + r_s}{R_\odot + r_s}\right)^{\Gamma - 3}, \qquad (2)$$

where Γ is the inner slope of the DM halo, and $\rho_\odot$ is the DM density at the position of the Solar System. Observational constraints from microlensing and rotation curves of stars or gas [58] on the slope of the DM halo in the inner few kpc of the Galaxy remain relatively weak and allow values up to $\Gamma \sim 1.5$. Throughout, we will use $\rho_\odot = 0.3$ GeV cm^{-3} and $r_s = 20$ kpc as reference values. Note that we are eventually only interested in the *ratio* of various constraints to the putative signal, implying that the local DM density $\rho_\odot$ drops out and thus can be fixed to any value simply as a matter of convention. In that case, the variation of the annihilation rate at the Sun's position corresponds to a variation of the annihilation cross section itself.

In Ref. [21], the authors find slopes $\Gamma \simeq 1.26 \pm 0.05$ (at 3σ C.L.) from an analysis of the inner Galaxy (excluding the inner one degree above and below the Galactic disk), and a value of $\Gamma \simeq 1.04$–1.24 from an analysis of the GC source. We will quote our main results using the central value of the inner Galaxy analysis, $\Gamma = 1.26$, and will comment on the impact of shallower profiles when necessary. Note that throughout the analysis, we will neglect the effect of substructure in the DM halo. Because of tidal forces, the associated boost at the GC is in general expected to be negligible; at kpc distances it can, however, lead to $\mathcal{O}(1)$ enhancements of the effective annihilation rate (see, e.g., Ref. [59]). Neglecting these effects renders our constraints conservative.

We show in Fig. 1 the radial dependence of the *DM annihilation rate per volume* for different values of Γ. The rates are normalized to yield an identical projected signal flux from the inner 1°–3° around the GC, taking $\langle\sigma v\rangle = 1.7 \times 10^{-26}$ cm^3 s^{-1} into $\bar{b}b$, $m_\chi = 35$ GeV and $\Gamma = 1.26$ as a benchmark.[1] For slopes Γ compatible with the GeV excess, and assuming a scale radius of $r_s = 20$ kpc, the annihilation rate can vary by a factor of ∼3.3 (namely, when taking $\Gamma = 1.24$ as reference, 2.9 up and 1.1 down).

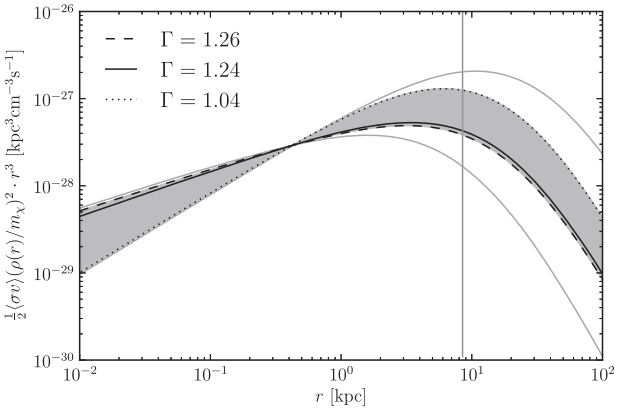

FIG. 1. DM annihilation rate per volume as a function of the galactocentric radius r, for different values of the inner slope Γ. The normalization is fixed to produce a signal emission in an annulus of 1°–3° around the GC that is compatible with the values quoted in Ref. [21] (see text for details). At the position of the Sun (vertical line) the annihilation rate can vary by a factor of 3.3, as indicated by the black lines. This region is extended as shown by the gray lines when allowing for variations in the scale radius of the DM profile, leading to an additional factor of 2 uncertainty in both directions. We multiplied the annihilation rate by r^3 for visual convenience.

Considering possible variations in the scale radius in the range $r_s = 20^{+15}_{-10}$ kpc, as suggested by DM-only simulations on the one hand and dynamical observations on the other hand (see discussion in Ref. [58]), allows for an additional change of up to a factor of 2 in the DM annihilation rate at the position of the Sun (see Fig. 1). Adopting the procedure discussed in Ref. [60] and requiring that a given DM profile with fixed $\rho_\odot$ and Γ can reproduce the Sloan Digital Sky Survey (SDSS) mass constraint $M(r = 60\,\text{kpc}) = 4.7 \times 10^{11} M_\odot$ [61], we find that $r_s = 24(34)$ kpc for $\Gamma = 1.0(1.26)$ if $\rho_\odot = 0.3$ GeV/cm^3, and $r_s = 15(18)$ kpc if $\rho_\odot = 0.4$ GeV/cm^3. Interestingly, these values favor the upper range of the above uncertainty band. Note that uncertainties in $R_\odot$ lead to variations in the annihilation rate at the Sun's position of at most a few 10%, which can be neglected in the present discussion.

Finally, Fig. 1 demonstrates that steepening the profile, by increasing Γ, makes local messengers (like positrons) a weaker probe of the GeV excess—while messengers originating from very small galactocentric distances (like radio signals) will lead to increasingly tighter constraints—and vice versa. Furthermore, constraints on the GC GeV

[1]We checked that normalizing instead in the range 1°–2° (1°–5°) would change the fluxes corresponding to $\Gamma = 1.04$ at most by +10% (−15%).

excess derived from observations at galactocentric distances of $\lesssim$100 pc (like our radio constraints) are practically independent of r_s. Combining information from indirect DM searches with different messengers thus allows one to test the DM hypothesis in a way that is even more independent of the assumed DM distribution than what can be inferred from gamma-ray observations alone.

The energy spectrum of the excess emission as derived from the inner Galaxy analysis of Ref. [21] can be well fitted with secondary photons from DM annihilation into hadronic final states. Fits with the harder photon spectra from annihilation into leptonic final states (caused by final state radiation and, in the case of τ leptons, the decay of energetic neutral pions) are, however, disfavored on purely statistical grounds with high significance. In case of annihilation into $\tau^+\tau^-$ final states, this discrepancy can be alleviated by adding a $\bar{b}b$ component of at least 20% (in which case the resulting $\Delta\chi^2$ is still worse by $\sim$20 than a pure $\bar{b}b$ fit). An alternative can be additional photons from bremsstrahlung and inverse Compton scattering [62]—though a sizable effect requires very large branching ratios into $e^\pm$ or $\mu^\pm$ final states, as, e.g., in the case of democratic annihilation to all leptons.

In Fig. 2, we show the values of the DM annihilation cross section and DM mass that are consistent with the GeV excess, based on the findings of Ref. [21]. We increased the size of the confidence regions to include the uncertainty in the DM profile slope—$\Delta\Gamma \simeq 0.05$ as inferred from the inner Galaxy analysis—in quadrature; this translates into a relative uncertainty of $\Delta\langle\sigma v\rangle/\langle\sigma v\rangle \simeq 22\%$. These numbers are also summarized in Table I for convenience and will be used as benchmarks in our subsequent study of implications for charged cosmic rays and radio emission. Furthermore, the vertical error bars indicate the range that is preferred by the GC analysis [21], which is in general higher than the range inferred from the inner Galaxy analysis.

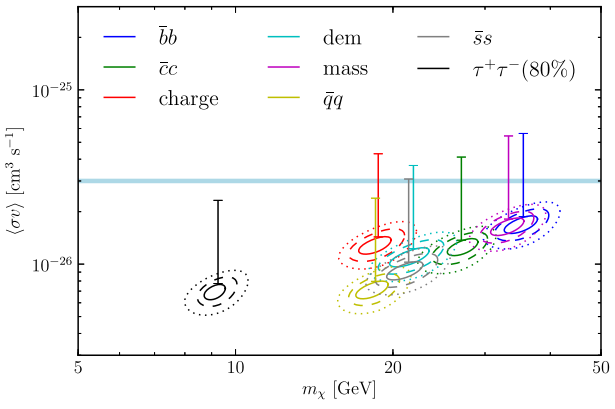

FIG. 2 (color online). The *ellipses* show the preferred values of the DM annihilation cross sections and mass from the inner Galaxy analysis of Ref. [21], where we include the uncertainties coming from the DM profile slope in quadrature ($\Gamma = 1.26 \pm 0.05$ at 3σ); see also Table I. The *error bars* indicate the annihilation cross section preferred for the values $\Gamma = 1.04$–1.24, as found from the GC analysis in Ref. [21].

TABLE I. List of benchmark annihilation channels that we consider in this work. Annihilation rates refer to a generalized NFW profile with central values $\Gamma = 1.26$ and local density $\rho_\odot = 0.3$ GeV/cm^3, using results from Ref. [21] (see there for a definition of final states). The errors are from the statistical fit (95% C.L.) and include additional uncertainties in $\Gamma = 1.26 \pm 0.05$ (3σ C.L.) in quadrature. Taking into account the larger uncertainties in the slope Γ as inferred from the GC analysis (see Fig. 1) can furthermore change the values as indicated in Fig. 2; for $\Gamma = 1.04$, e.g., the best-fit value of $\langle\sigma v\rangle$ given in the table must be multiplied by 3.3.

Channel	Mass m_χ [GeV]	Cross section $\langle\sigma v\rangle$ [10^{-26} cm^3 s^{-1}]
$\bar{b}b$	35.5 ± 4.2	1.7 ± 0.3
$\bar{c}c$	27.0 ± 3.3	1.2 ± 0.22
$\bar{q}q$	18.5 ± 2.1	0.72 ± 0.13
$\tau^+\tau^-(80\%)$	9.3 ± 0.8	0.7 ± 0.12
Mass	33.3 ± 3.9	1.6 ± 0.29
Dem	21.9 ± 3.1	1.1 ± 0.2
$\bar{s}s$	21.4 ± 2.9	0.93 ± 0.16
Charge	18.7 ± 2.3	1.3 ± 0.23

B. Astrophysical scenarios

For completeness, we will here briefly sketch astrophysical scenarios that might account for the excess emission seen at the GC. The arguably most plausible explanation for at least part of the observed excess emission at and close to the GC is the emission from a large number ($\sim$1000) of MSPs below the point-source sensitivity of Fermi-LAT [49]. Up to now, more than 40 MSPs have been observed in gamma rays by the Fermi-LAT [63], with spectra that are compatible with the spectrum of the extended source at the GC [54] (unless the spectrum of the GC excess below 1 GeV is confirmed to be extremely hard [21]). MSPs remain gamma-ray emitters for billions of years, and it was argued that with kick velocities of the order of $\sim$40 km/s they have the right properties to in principle account for the steepness as well as the extension of the observed gamma-ray excess [24]. The main argument against a significant contribution of MSPs to the GC excess is that it appears to be nontrivial to find plausible source distributions that completely remain below the Fermi-LAT point source threshold [64–66], while still being compatible with the emission properties of the pulsar population that is observed locally.

The emission of TeV gamma rays in the Galactic ridge region as observed by H.E.S.S. (in the inner $|b| < 0.3°$ and $|\ell| < 0.8°$) is well correlated with the distribution of molecular clouds that are observed in the inner 200 pc around the GC by means of radio observations [67]. This strongly suggests that the diffuse TeV gamma-ray emission

is due to a hard population of cosmic-ray electrons or protons, producing gamma rays via either bremsstrahlung or proton-proton interactions. It is plausible that the same populations also contribute to the GC emission at GeV energies. In the context of cosmic-ray electrons, Ref. [52] showed that the bremsstrahlung from an electron population compatible with the observed synchrotron emission at the GC could indeed produce the characteristic peaked GeV excess emission. The main argument against the interpretation in terms of cosmic rays is the apparent extension of the GeV excess to ∼kpc distances from the GC as well as its spherical symmetry, which does not resemble the distribution of detected gas (see, e.g., Ref. [27]). Recent counterexamples that go beyond the typical assumptions of static cosmic-ray equilibrium at the Galactic center were presented in Refs. [68,69]. In both papers, the authors discuss recent burst events (up to about 1 million years ago) that injected either high-energy electrons [68] or protons [69] at the Galactic center, giving after a diffusion period rise to a quasispherical excess emission around the GC.

III. CONSTRAINTS FROM OTHER INDIRECT DETECTION CHANNELS

We now turn to a discussion of other messengers for the indirect detection of DM than gamma rays. In all these cases the source function is given by the differential injection rate of particles from DM annihilation, $Q(r, E) = \frac{1}{2}\langle\sigma v\rangle dN/dE(\rho_\chi/m_\chi)^2$, that was already introduced in Eq. (1) in the context of gamma rays. As stressed in the previous section (cf. Figs. 1 and 2), this quantity is rather tightly constrained if the GeV excess is indeed explained by DM. In consequence, the intrinsically large uncertainties associated to the DM distribution by which limits from indirect detection are typically hampered are greatly reduced in our case. In particular, they do not depend on the overall normalization of the DM density profile (conventionally expressed in terms of the local DM density $\rho_\odot$).

The spectrum of the DM signal is determined by dN/dE, i.e., the differential number of a given species of cosmic-ray particles that are produced per annihilation. We obtain these functions from DarkSUSY 5.1.1 [70], which provides tabulated fragmentation functions for various possible annihilation channels based on the event generator PYTHIA 6.414 [71] (for light quarks $q = u$, d, s, we take instead the spectra provided in Ref. [60] as those are currently not implemented in DarkSUSY).

A. Antiprotons

Final state quarks from DM annihilation in the Galaxy will fragment and produce antiprotons [72]. Unlike gamma rays, those are deflected by stochastically distributed inhomogeneities in the galactic magnetic field such that the resulting propagation can be modeled by a diffusion process [73]. On the other hand, there are no primary but only secondary sources of astrophysical antiprotons: these are produced through the collisions of cosmic rays, in particular protons, with the interstellar medium. This astrophysical background is extremely well understood and can nicely be described in relatively simple semi-analytical diffusion models with cylindrical symmetry [74,75]. Fitting the parameters of those models to *other* cosmic-ray data, in particular other observed secondary to primary ratios like the boron over carbon ratio B/C [76], results in a prediction for the antiproton background that is tightly constrained and provides a very good fit to the data.

The main uncertainty in the background prediction derives from the range of propagation parameters compatible with B/C and from uncertainties in the nuclear cross sections for the production of antiprotons. For the energy range we are interested in here, both effects can independently affect the flux by up to about 30% [73]. For recent studies that find similar values, and offer more detailed discussions about the underlying systematics, see Refs. [77,78]. In our analysis, we will take into account the full range of uncertainty in the background prediction by two independent parameters $\alpha_{\rm prop}$, $\alpha_{\rm nuc} \in [0, 1]$ that interpolate linearly between the minimal and maximal predictions for the secondary flux due to these two effects (for which we use the results from Refs. [74] and [75], respectively). Low-energy antiprotons are furthermore affected by local effects like adiabatic energy losses in the expanding solar wind and diffusion in the solar magnetic field, often collectively referred to as solar modulation (see, e.g., Ref. [79] for a recent discussion). For the energies of interest to our analysis this is extremely well described by the force-field approximation [80,81] (see discussion in Sec. IV A), implying that a single parameter—the Fisk potential ϕ_F—is sufficient to relate the local interstellar (LIS) antiproton flux to the one measured at the top of the atmosphere (TOA).

For our analysis we use the newest release of PAMELA data that result from measurements between June 2006 and January 2010 [82], featuring significantly reduced error bars with respect to any previous antiproton data.[2] These data agree remarkably well with the much older predictions [74] for the antiproton background we are testing against: with the three free parameters described above, we find $\chi^2/\text{d.o.f.} = 10.1/(23-3) = 0.51$ for the best fit point. Clearly, this provides an important test for the underlying diffusion model. In Fig. 3 we plot this best-fit prediction for the background as a solid line, along with the PAMELA data points. The yellow band in that figure corresponds to a choice of nuclear cross section parametrization that

[2]Note that the error bars stated in that data release are statistical only. Systematical error bars are expected to be of the same order as in the first release [83] of PAMELA data [84]. In our analysis, we thus add those in quadrature.

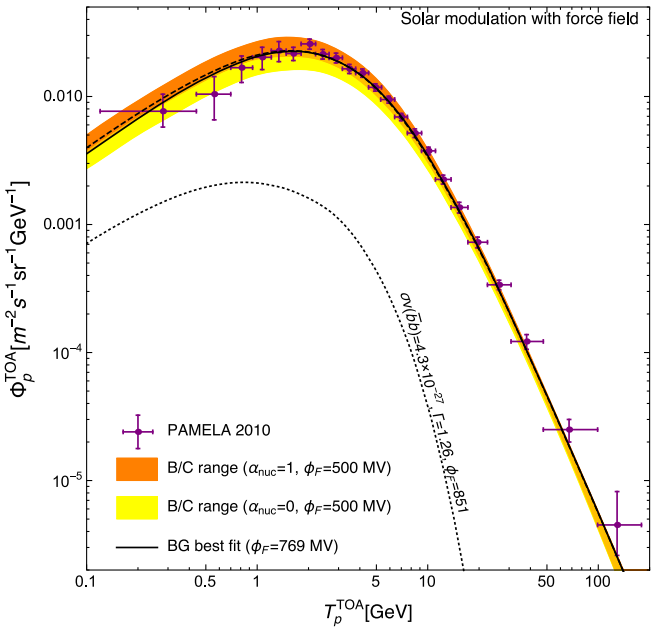

FIG. 3 (color online). PAMELA antiproton data [82] as measured on top of the atmosphere (TOA). The colored bands show the prediction for the astrophysical background (BG), with the width of each band deriving from uncertainties in the propagation parameters left from the B/C analysis. The two different bands bracket the uncertainty from nuclear cross sections, where the maximal (minimal) flux corresponds to the analysis performed in Ref. [75] ([74]). The best-fit BG model is given by the solid line. For comparison, the dotted and dashed lines also show the case of a fiducial WIMP with mass 34 GeV, annihilating to $\bar{b}b$ with a rate barely allowed at 95% C.L. (see Fig. 4).

minimizes the flux (as adopted in Ref. [74], this corresponds to setting $\alpha_{\rm nuc} = 0$ in our analysis), while the orange band corresponds to a choice that maximizes the flux (as in Ref. [75], corresponding to our $\alpha_{\rm nuc} = 1$). In both cases, the width of these bands is given by the uncertainty in the propagation parameters that results from the B/C analysis (which corresponds to varying our parameter $\alpha_{\rm prop}$ from 0 to 1).

The contribution to the antiproton flux from DM annihilation [72] is subject to much larger theoretical uncertainties than what is illustrated by the colored bands in Fig. 3 for the astrophysical background [85]. The main reason for this is that DM annihilation is very efficient in a rather large part of the halo, implying that it probes a much larger volume of the diffusion zone than the B/C analysis that is restricted to sources in the Galactic disk. In particular, the antiproton flux from DM is mostly sensitive to the thickness L of the diffusion zone perpendicular to the Galactic plane, while B/C essentially only constrains the *ratio* of L and the diffusion coefficient D [86]. While the B/C analysis in principle allows a diffusion zone as small as $L \sim 1$ kpc, a vertical extension of $L \sim 10$ kpc is preferred when taking into account radioactive isotopes [87], with similar results obtained when adding gamma rays [88,89] and cosmic-ray electrons [90,91] to the analysis. Also radio [92,93] and low-energy cosmic-ray positron [94] data have been shown to be clearly inconsistent with a halo size as small as ~1 kpc. With this in mind, we will in the following mainly use the recommended reference model, "KRA," of the recent comprehensive analysis presented in Ref. [95], which features $L = 4$ kpc (and is very similar to the best-fit model of Ref. [86]). For the propagation of primary antiprotons we use DARKSUSY [70], which implements the semianalytical solution of the diffusion equation described in Refs. [95,96].

We use the likelihood ratio test [97] to determine limits on a possible DM contribution to the antiproton flux measured by PAMELA. For the likelihood function, we adopt a product of normal distributions over each data bin i,

$$\mathcal{L} = \Pi_i N(f_i|\mu_i, \sigma_i), \tag{3}$$

where f_i is the measured value, μ_i the total antiproton flux predicted by the model and σ_i its variance. For a given mass and annihilation channel, the DM contribution enters with a single degree of freedom that parametrizes the non-negative signal normalization (and which we will always express in terms of the annihilation rate). The 95% C.L. upper limits on $\langle\sigma v\rangle$ are thus derived by increasing the signal normalization from its best-fit value until $-2\ln\mathcal{L}$ has changed by 2.71, while refitting ("profiling over") the parameters $(\alpha_{\rm prop}, \alpha_{\rm nuc}, \phi_F)$ of the background model.

In Fig. 4, we show the resulting limits on $\langle\sigma v\rangle$ as a function of the DM mass m_χ, for all quark final states and two representative values of the Γ parameter of the generalized NFW profile of Eq. (2). Limits for the standard NFW profile ($\Gamma = 1$) are essentially indistinguishable from the $\Gamma = 1.04$ case displayed here. These limits are one of our main results and rather strong, excluding the cross section $\langle\sigma v\rangle_{\rm therm} \equiv 3 \times 10^{-26}$ cm^3 s^{-1} typically favored by thermally produced DM up to masses of $m_\chi \sim 35$–55 GeV for an NFW profile (depending on the channel). There are two main reasons why we could improve previous limits [79,95,98,99] by a factor of roughly 2–5 at the DM masses of interest here (while the limits presented in Ref. [100] are actually slightly *stronger* than ours): (i) we use the only recently published update of PAMELA data [82] rather than the first public release [83], and (ii) we employ an improved statistical treatment of the background uncertainties (see Sec. IV A for a more detailed discussion).[3] When comparing these results to Fig. 2, we find that any interpretation of the gamma-ray excess as being due to DM annihilating into quark final states is in strong tension with the cosmic-ray antiproton data.

[3]Below $m_\chi \sim 50$ GeV, the limits presented in Ref. [99] become furthermore significantly weaker due to the deliberate choice of not including data with $T < 10$ GeV.

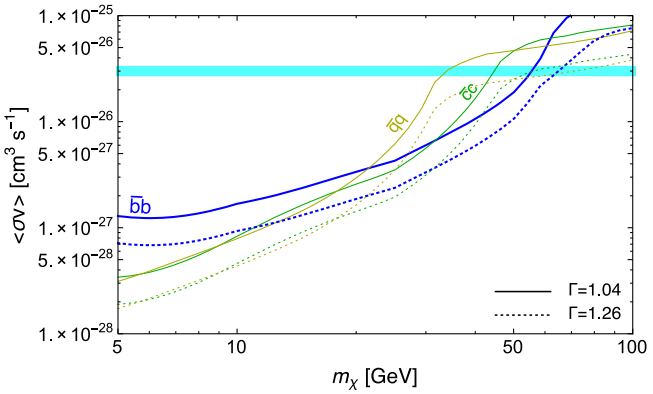

FIG. 4 (color online). Limits on the annihilation rate of DM into quark final states from our analysis of the PAMELA antiproton data. Solid lines refer to the generalized NFW profile of Eq. (2) with $\Gamma = 1.04$ and are essentially indistinguishable from the standard NFW ($\Gamma = 1$) case; dotted lines show the case for $\Gamma = 1.26$.

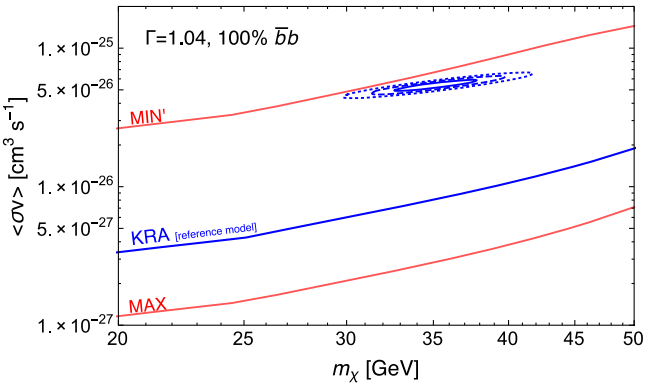

FIG. 5 (color online). Reference $\bar{p}$ limits (thick line) and effects of varying the propagation scenario for $\bar{b}b$ final states. As in Fig. 4, the area above the lines is excluded at 95% C.L. For comparison, also the signal region for a DM interpretation of the gamma-ray excess in the inner Galaxy [21] is plotted, rescaled to $\Gamma = 1.04$.

Let us, finally, comment on the impact of different propagation scenarios on our limits. Conventionally, the corresponding uncertainty is bracketed by two sets of propagation parameters, "MIN" and "MAX," that are consistent with the B/C analysis and, respectively, minimize and maximize the primary antiproton flux from DM annihilation [85]. As we have stressed before, however, there are several additional observations that constrain these parameters much better than the B/C analysis alone, such that the range of allowed fluxes spanned by MIN and MAX must be considered unrealistically large. To give a conservative indication of the involved astrophysical uncertainties, and to follow the typically adopted procedure, we still show in Fig. 5 how our limits change when varying the propagation parameters within these ranges.[4] As can be seen from this figure, the DM interpretation of the excess becomes compatible with limits from the PAMELA antiproton data only in the most unfavorable case of propagation parameters—at least within the cylindrical two-zone diffusion model that is commonly considered. Antiproton data from the AMS-02 experiment on board of the international space station may improve limits on a DM contribution by as much as 1 order of magnitude with respect to the current PAMELA data [79,95,99]. Expected to be published in less than a year from now, AMS-02 data will thus either show an excess also in antiprotons or allow one to rule out the DM hypothesis with rather high confidence. Similar conclusions apply more generally to other quark annihilation channels and DM profiles than what is shown explicitly in Fig. 5 (i.e., $\bar{b}b$ and $\Gamma = 1.04$).

[4]Given that $L = 1$ kpc as featured by the MIN model proposed in Ref. [85] has in the meantime been firmly ruled out, however, we used instead a MIN' model with the same parameters as MIN but with $L = 2$ kpc and a diffusion coefficient of $D_0 = 9.65 \times 10^{26}$ cm^2 s^{-1}. This takes into account the lower bound of $L \geq 2$ kpc from radio observations [92,93] and the fact that B/C only is sensitive to L/D_0 [76,86]. Note that even $L = 2$ kpc is very conservative in light of the recent analysis of low-energy positron data [94].

B. Positrons

The energy spectrum of cosmic-ray positrons as well as the *positron fraction* (the fraction of positrons in the total electron and positron flux) was recently measured with unprecedented precision by the AMS-02 [101] experiment, in the energy range 0.5 to 350 GeV. AMS-02 confirmed the rise in the positron fraction at energies above 10 GeV that was previously observed by PAMELA [102] and Fermi-LAT [103], but with significantly smaller statistical and systematical errors. This allowed for the first time a dedicated spectral search for signals from light ($m_\chi \lesssim$ 350 GeV) DM particles annihilating into leptonic final states [104,105], in a way that is largely independent of the origin of the rise in the positron fraction itself. For DM masses around 10 GeV, the limits on the annihilation cross section into e^+e^- ($\mu^+\mu^-$) are very tight and around 1.2×10^{-28} cm^3 s^{-1} (1.3×10^{-27} cm^3 s^{-1}) [104].

The AMS-02 measurements of the positron fraction have important consequences for the DM interpretation of the GeV excess. We will here consider the option that the GeV excess is dominantly caused by annihilation into leptonic two-body final states, with a possible admixture of $\bar{b}b$. This scenario is described by the branching ratios into the three charged lepton families (e^+e^-, $\mu^+\mu^-$, and $\tau^+\tau^-$ final states) as well as $\bar{b}b$. For a given set of branching ratios, we calculate the prompt gamma-ray emission using DarkSUSY [70]. We refit the energy spectrum of the GC excess emission (Fig. 5 in Ref. [21]) to obtain the total annihilation cross section and DM mass, assuming a DM profile with $\Gamma = 1.26$. During the fit, we constrain the DM mass to be larger than 9.2 GeV to approximately account

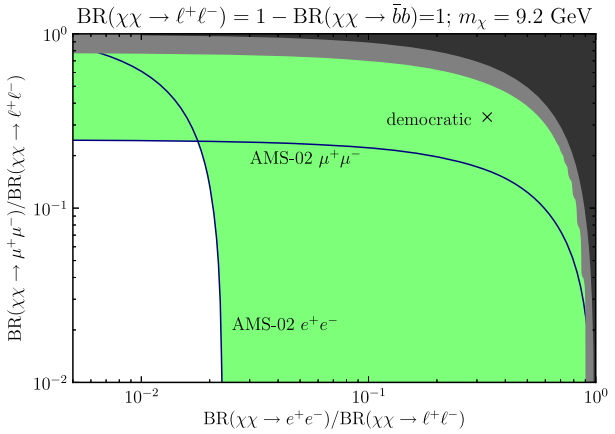

FIG. 6 (color online). Upper limits (95% C.L.) on the relative branching ratios into leptonic two-body final states, as derived from a spectral analysis [104] of AMS-02 positrons. We assume 100% annihilation into leptonic final states. For each point, we determine the DM mass and cross section by a fit to the gamma-ray spectrum of the inner Galaxy excess [21], assuming $\Gamma = 1.26$. The green regions are excluded, while the gray region shows where the spectral fit to the GeV excess worsens significantly (see text for details). The white area shows the remaining allowed parameter space, corresponding to an almost pure $\tau^+\tau^-$ final state. Note, however, that this gives a fit to the data that is still much worse (by about $\Delta\chi^2 \sim 130$) than a fit with a $\bar{b}b$ final state.

for the fact that bremsstrahlung and inverse Compton emission can potentially contribute at low energies to reconcile the spectra of mixed leptonic final states with the measurements [62] (though this argument only works in the case of sizable branching ratios to e^+e^- final states, as is the case for the democratic scenario that Ref. [62] considers).

For a given set of branching ratios and the implied DM mass and total cross section, we adopt the AMS-02 limits from Ref. [104] to decide whether a scenario is excluded. We use here the central values of the limits from Ref. [104]; uncertainties in the local radiation field allow these limits to weaken by maximally a factor of 2. We use a reference value of $\Gamma = 1.26$ throughout. Note that a shallower profile would strengthen the AMS-02 limits, which mostly depend on the annihilation rate at the Sun's position, by a factor of $\sim$3; variations in the scale radius r_s allow for an additional factor of 2 up or down in the annihilation rate (cf. Fig. 1).

The results of this procedure are shown in Figs. 6 and 7: In Fig. 6 we consider the purely leptonic case, i.e., $\mathrm{BR}(\chi\chi \to \bar{b}b) = 0$. In this figure, the best-fit DM mass always stays close to the imposed lower limit of 9.2 GeV. The white areas are allowed and the green areas excluded by limits on e^+e^- or $\mu^+\mu^-$ final states at 95% C.L.; the gray area indicates where the formal fit to the data becomes worse by $\Delta\chi^2 \gtrsim 25$. In Fig. 7 we show the same situation, but assume that 20% (left panel) or 80% (right panel) go into $\bar{b}b$ final states. In each case, we indicate in the figure header the best-fit mass that we obtain in the limit $\mathrm{BR}(\chi\chi \to \mathrm{e^+e^-}) = \mathrm{BR}(\chi\chi \to \mu^+\mu^-) = 0$. As one can see from these plots, the democratic case, featuring equal leptonic branching ratios, is clearly excluded from AMS-02 cosmic-ray positron data.

Let us stress again that leptons alone do not feature a spectral shape consistent with that of the GeV excess. This holds not only for the extremely hard spectrum associated with light lepton final states, but also for the slightly softer spectrum from tau leptons. Because of the strong AMS-02 constraints on the contribution from $\mu^\pm$ and $e^\pm$ final states for $\mathrm{BR}(\chi\chi \to \bar{b}b) \lesssim 0.2$, we find that this conclusion cannot be changed by including the effect of inverse Compton and bremsstrahlung processes, as suggested in Ref. [62]. Note that this holds even if annihilation is assumed to happen dominantly into $\mu^\pm$ and $\tau^\pm$, thereby evading the extremely strong constraints for $e^\pm$ final states: To produce a reasonable fit to the data, one would in that case need $\mathrm{BR}(\chi\chi \to \mu^+\mu^-) \gg 0.25$ [62], which we identify in Fig. 6 as being excluded by AMS-02 data.

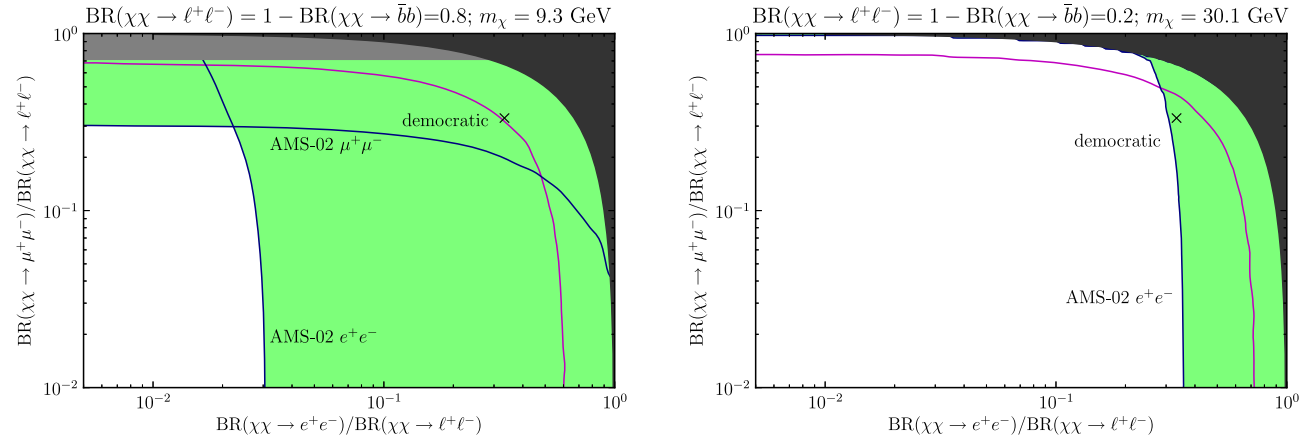

FIG. 7 (color online). Same as Fig. 6, but for nonzero branching ratios into $\bar{b}b$ final states. The magenta line in the left (right) panel indicates where the best-fit DM mass exceeds 14 (34) GeV.

C. Radio signals

Electrons and positrons from DM annihilation (henceforth collectively referred to as electrons) are expected to emit synchrotron radiation when propagating through the Galactic magnetic fields. Here, we shall focus on corresponding radio signals from the GC. In particular, we will use the Jodrell Bank upper flux limit of 50 mJy from this region [106], obtained for a frequency of 408 MHz, to constrain the DM annihilation rate. As has been noticed before [107–115], the resulting constraints are typically rather strong. In this subsection we will derive our baseline constraints and defer a critical discussion of the steps to Sec. IV C.

The arguably most critical—yet, as we shall see, realistic—assumption that enters our analysis is that the electrons in the GC region lose their energy essentially *in situ*, via synchrotron radiation, implying that both free-streaming and diffusion effects can be neglected. This is motivated by the fact that one expects a much larger turbulent magnetic field at $\mathcal{O}(1\ \mathrm{pc})$ distances from the GC [116] than the average Galactic value of $\sim 6\ \mu$G [117]. To get a quantitative idea of the magnetic field strength that is required, we will here assume that diffusion at $\lesssim 1$ pc from the GC is well described by Bohm diffusion (see Ref. [108] for a similar treatment); in Sec. IV C we will argue that this assumption can in fact be relaxed by several orders of magnitude. In the case of Bohm diffusion, the scattering length of the diffusion process is given by the gyroradius r_g, leading to a diffusion constant ($D_{\mathrm{Bohm}} = \frac{1}{3} r_g c = E_e c/3eB$). The length scale $l_{\mathrm{diff}} \simeq (D_{\mathrm{Bohm}} t_{\mathrm{loss}})^{1/2}$ over which relativistic electrons propagate during their synchrotron energy loss time, $t_{\mathrm{loss}} \approx E/b(r,E) = 3m_e^4 c^7/2e^4 B^2 E$ where $b(r,E)$ is the loss rate, should then be significantly smaller than the DM density scale height $l_\chi \equiv |\rho_\chi(r)/\rho'_\chi(r)|$, i.e., [115]

$$\frac{l_{\mathrm{diff}}}{l_\chi} \simeq \frac{m_e^2 c^4}{\sqrt{2} e^{5/2} l_\chi B^{3/2}} \lesssim 1. \tag{4}$$

For the generalized NFW profile that we consider here, see Eq. (2); this implies a lower limit on the magnetic field strength of

$$B(r) \gtrsim 4\Gamma^{2/3} \left(\frac{\mathrm{pc}}{r}\right)^{2/3} \mu\mathrm{G} \tag{5}$$

for the diffusion of electrons from DM annihilation at the GC to be negligible. Once this condition is satisfied, the resulting limits will actually *decrease* with increasing B (while the opposite is true in the regime where diffusion cannot be neglected; see, e.g., Ref. [118]).

Observationally, the magnetic field in the Galaxy can be inferred only indirectly via the Faraday effect. The resulting rotation of polarized radio waves with wavelength λ is given by $\beta = \lambda^2 \times \mathrm{RM}$, where the *rotation measure* (RM) is proportional to the integral over the line-of-sight magnetic field $B(r)$ and the electron density $n(r)$, $\mathrm{RM} \propto \int B(r) n(r)$.

At the distances that are of interest for our radio discussion, ~ 0.1 pc, Ref. [119] infers the magnetic field from multiwavelength observations of the recently discovered magnetar PSR J1745-2900, which has a rotation measure of $\mathrm{RM} \sim 7 \times 10^4\ \mathrm{rad\,m^{-2}}$ at a projected distance of 0.12 pc from the central black hole, Sagittarius A* (Sgr A*).[5] Together with an observed dispersion measure of $\sim 1.8 \times 10^3\ \mathrm{cm^{-3}\,pc}$, which determines the column density of electrons toward the pulsar, this allows one to derive a very conservative lower limit on the magnetic field of 50 μG (assuming that all electrons along the line-of-sight are localized close to the Galactic center, and that no turbulent field components and/or field reversals reduce the RM). A more realistic estimate gives a much larger lower limit of about 8 mG [119], but it is interesting to note that already the extremely conservative limit satisfies Eq. (5) if Bohm diffusion is realized.

For definiteness, we follow the often adopted assumption [116] that the magnetic field near the Galactic center is mainly powered by the central SMBH. Concretely, this means that we assume an approximate equipartition of magnetic, kinetic, and gravitational energy inside the accretion zone, i.e., $B \propto r^{-5/4}$ for $r < R_{\mathrm{acc}} = 0.04$ pc (see also Refs. [121,122]). For $r > R_{\mathrm{acc}}$, which is the region most relevant for our limits, magnetic flux conservation leads to $B \propto r^{-2}$. In Fig. 8, we plot this magnetic field profile [111] along with the condition given in Eq. (5) and the observationally inferred lower limits.

If energy losses are dominated by synchrotron radiation, and the effect of diffusion can be neglected, the transport equation can be solved analytically. The total synchrotron flux density is then given by [108,111,115]

$$F_\nu \simeq \frac{\langle \sigma v \rangle}{8\pi \nu R_\odot^2 m_\chi^2} \int E \rho_\chi^2(r) N_e(E) \mathrm{d}V, \tag{6}$$

where $N_e(E)$ denotes the number of electrons (or positrons) per annihilation, with energy larger than E. In arriving at this expression, the monochromatic approximation for synchrotron radiation was used,

$$E = \left(\frac{4\pi m_e^3 \nu}{eB}\right)^{\frac{1}{2}} = 0.46 \left(\frac{\nu}{\mathrm{GHz}}\right)^{\frac{1}{2}} \left(\frac{B}{\mathrm{mG}}\right)^{-\frac{1}{2}} \mathrm{GeV}, \tag{7}$$

which we checked affects our limits by less than 30% for the masses of interest here. The integration volume in Eq. (6) is a cone corresponding to the 4" region

[5]For comparison, the highest RM of *any* Galactic source, $\sim 5 \times 10^5\ \mathrm{rad\,m^{-2}}$, is associated with the radio emission of Sgr A* itself [120].

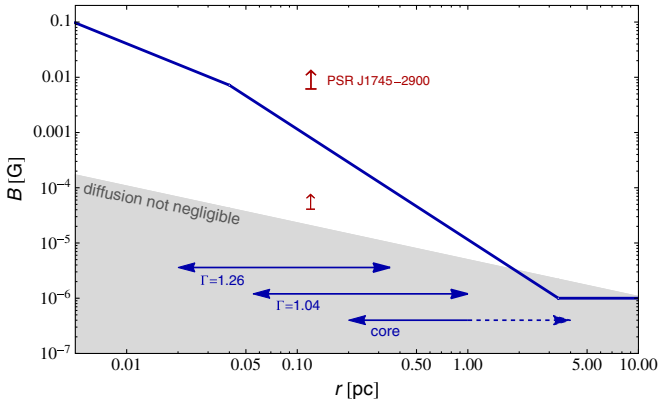

FIG. 8 (color online). *Solid line*: Simplified model for the magnetic field profile close to the GC black hole [111], assuming energy equipartition inside the accretion volume and magnetic flux conservation outside. The *gray area* defines the domain where Bohm diffusion can no longer be neglected [as assumed in our analysis; cf. Eq. (5)]. Lower limits (in red) refer to ultraconservative and realistic field values, respectively, inferred from multiwavelength observations of the recently discovered magnetar PSR J1745-2900 [119]. Horizontal arrows indicate the ranges of galactocentric distances that, depending on the profile, contribute ~95% of the annihilation signal flux at 408 MHz in the 4" cone observed in Ref. [106] (see text for details). For our actual limits, we conservatively take only radio fluxes from the inner 1 pc around the GC into account.

(~0.32 pc of diameter at the GC) observed at Jodrell Bank [106]. We restrict the integration to a region $r < r_{\rm max} = 1$ pc where diffusion can be safely neglected (see Fig. 8), thus ignoring the synchrotron emission of electrons created in regions where diffusion effects are not clearly negligible. While this restriction has no significant effect on our limits for the case of a generalized NFW profile, it renders our limits in the presence of a core, as discussed below, rather conservative.

In Fig. 9 we show the results from confronting the DM hypothesis with the 408 MHz Jodrell Bank upper limit in the case where the annihilation of DM particles occurs with a branching ratio of 80% into $\tau^+\tau^-$ and with 20% into $\bar{b}b$. Besides limits for a generalized NFW profile with $\Gamma = 1.26$ (left panel) and $\Gamma = 1.04$ (right panel), we also show limits for these profiles if an *ad hoc* cutoff at a galactocentric distance r_c is introduced in the DM density profile. Below this, the DM density is assumed to stay constant, i.e., $\rho_\chi(r < r_c) = \rho_\chi(r_c)$ while $\rho_\chi(r > r_c)$ is given by Eq. (2). At much smaller scales than considered here, such a DM density plateau is expected to result from the large DM annihilation rate [123] (in extreme cases, also dynamical effects like the off-center formation of the SMBH [124] or major SMBH merger events [125] could significantly reduce the DM density at $r \lesssim 1$ pc, though this would not result in a complete flattening of the profile). Here, the postulated flattening at $r < r_c$ rather serves as a phenomenological parametrization of the maximal effect that uncertainties in the DM distribution at small scales may have on our limits. Let us stress that the DM interpretation of the GeV excess fixes the form of the density profile down to roughly 10 pc [21], and that there is no particular reason to *expect* a cutoff at only slightly smaller scales. GC radio observations thus place extremely tight constraints on annihilating DM for the steep density profiles considered here, at least if extending down to $r > r_c \sim 1$ pc.[6] In fact, as we will discuss in more detail in Sec. IV C, these limits generally depend much more strongly on the DM profile—which is fixed once we accept the DM interpretation of the GeV excess—than on the strength of the magnetic field.

In Fig. 10, we finally compare our radio limits directly to the gamma-ray signal claims [21] for various annihilation channels. Assuming that the observed profile extends down to a moderate $r_c \lesssim 2$ pc, indeed, we find that *all* channels are excluded as an explanation of the signal. Here, we used an inner slope of the DM profile of $\Gamma = 1.04$; increasing this to $\Gamma = 1.26$ would tighten the limits by roughly 1 order of magnitude for the DM masses that best describe the excess.

For completeness, let us mention that a standard NFW profile ($\Gamma = 1$) without a core, or a core at galactocentric distances less than 0.1 pc, leads to limits that are less than a factor of 3 weaker than for the case of $\Gamma = 1.04$ considered above. This implies that for such a profile thermal cross sections are excluded for DM masses below roughly 120 GeV (400 GeV) for $\tau^+\tau^-$ ($\bar{b}b$) final states. For an Einasto profile, on the other hand, we find constraints that are weaker by more than 2 orders of magnitude below $m_\chi \sim 100$ GeV, thus not probing thermal cross sections even for dark matter masses as small as a GeV. This large difference is easily understood by observing that for the small distance scales $r \sim 1$ pc that are most relevant in setting the limits (cf. Fig. 8), the Einasto profile is already much shallower than the NFW profile.

D. Further constraints

Strong and robust constraints on light annihilating DM particles are in principle also provided by measurements of the *cosmic microwave background* (CMB) [126–131]. However, even projected limits from Planck data [130] for light lepton final states are much less constraining than the AMS-02 positron limits discussed above (and somewhat weaker for τ lepton final states). For quark final states, it will be possible to probe the thermal annihilation cross section up to masses of ~25 GeV. While this provides

[6]It is worth stressing that for such large core sizes, $r_c \gtrsim 1$ pc, the limits shown in Fig. 9 are rather strongly affected by our conservative choice of restricting the volume for which we consider synchrotron integration. Changing the integration range in Eq. (6) from $r < r_{\rm max} = 1$ pc to $r_{\rm max} = 4$ pc inside the 4" cone, for example, the constraints depicted for the $r_c = 10$ pc case would tighten by a factor of up to a few for $m_\chi = \mathcal{O}(10)$ GeV.

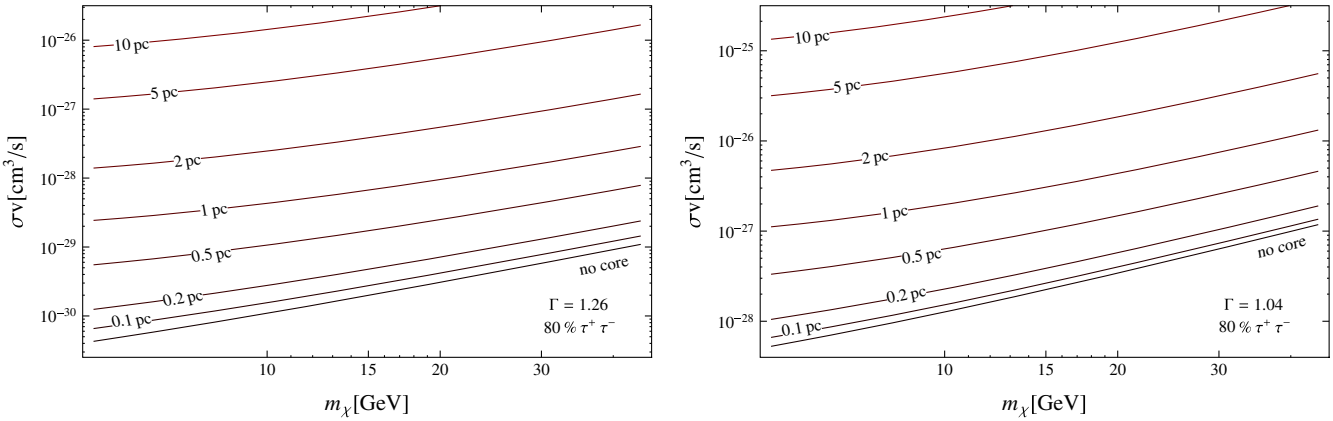

FIG. 9 (color online). *Left panel*: Limits from radio observations on the annihilation rate of DM particles into 80% $\tau^+\tau^-$ and 20% $\bar{b}b$, for a generalized NFW profile with an inner slope of 1.26 (lowest line). The other curves show the same limits when adding an artificial core to the DM profile with a core size r_c as indicated (i.e., assuming a constant profile for galactocentric distances smaller than what is stated next to the respective curve). *Right panel*: same as left panel but with an inner slope of $\Gamma = 1.04$.

interesting and completely complementary limits compared to the ones derived from cosmic-ray antiproton observations, this only barely starts to constrain the assumed GeV signal region for DM annihilation into light quarks (cf. Fig. 2).

Gamma-ray observations of dwarf spheroidal galaxies of the Milky Way are a further powerful and robust probe for the annihilation of DM. As practically background-free targets, and with a DM content that is well constrained from observations of member stars, they were used by several groups to perform DM searches both with space- and ground-based telescopes [132–138]. For light DM, the most recent study was based on a combined analysis of

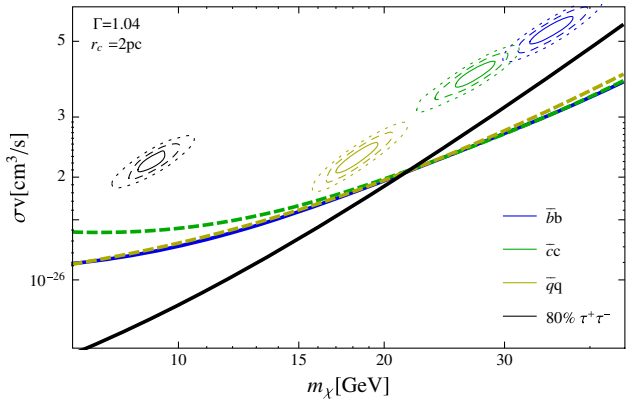

FIG. 10 (color online). Constraints from GC radio observations for various annihilation channels, along with the corresponding contours characterizing the DM interpretation of the GeV excess in gamma rays [21]. These constraints assume an *ad hoc* core in the DM density profile at galactocentric distances smaller than $r_c = 2$ pc, i.e., only slightly below the $\mathcal{O}(10)$ pc distance down to which the signal profile is observed in gamma rays (see Fig. 9 for an indication of how limits improve if the profile is assumed to continue to smaller scales).

Fermi-LAT observations of 15 dwarf spheroidal galaxies [133]. Only upper limits on the annihilation cross section of DM could be found, and in case of, e.g., $\chi\chi \to \bar{b}b$, these are consistent with the DM interpretation of the GeV excess at the Galactic center. Interestingly, however, for DM masses around $m_\chi = 10$–25 GeV the current analysis indicates a slight preference for a signal at $\sim 2.3\sigma$ (after the typical fluctuation level of the extragalactic gamma-ray background has been taken into account). Data collected by the Fermi-LAT over the upcoming years will help to sort out whether this is a signal or merely a fluctuation.

Constraints from galaxy clusters [139–142] or the extragalactic gamma-ray background [143,144] are less stringent, since they rely heavily on the distribution of substructures in DM halos. However, a cross-correlation between the distribution of DM in the local Universe and the unresolved gamma-ray sky can be a promising venue to confirm the GeV excess at higher latitudes [145–149]. In passing, let us mention that previous constraints derived from GC observations [100,150] are actually somewhat in tension with the observed GeV excess and its interpretation in terms of DM annihilation.

Radio searches for DM annihilation have recently been performed also for other targets than the GC that we have discussed at length above. The goal is usually not to identify a DM signal—which is extremely hard due to the large modeling uncertainties of signals and backgrounds—but to put upper limits on the DM annihilation rate. In contrast to the constraints derived in the present work, which only depend weakly on the magnetic field, above a certain threshold, most other constraints critically depend on the assumptions about magnetic field and cosmic-ray diffusion. Limits and prospective constraints from the inner Galaxy (a few degrees off the GC) were discussed in Refs. [113,114,151–153]. The most recent analysis of Galaxy clusters was presented in Ref. [154],

leading to limits that are stronger than corresponding cluster constraints from gamma-ray observations. Radio searches in dwarf spheroidal galaxies suffer from the basically unknown magnetic field in dwarfs [155,156].

The Andromeda galaxy (M31), on the other hand, has currently a lower star formation rate than the Milky Way, making it particularly suited for radio searches for DM. For realistic assumptions about the magnetic field, recent searches in M31 lead to very competitive constraints [157]. Depending also on the assumed halo model of M31, these are in some tension with the DM interpretation of the GeV excess.

IV. DISCUSSION

In the previous section we have seen that indirect searches using other messengers than gamma rays place very strong constraints on light annihilating DM, essentially for every possible fermionic annihilation channel (with the exception of neutrinos, which we have not discussed here). These constraints, if taken at face value, have far-reaching implications for a possible DM interpretation of the GeV gamma-ray excess. In this section, we will therefore reassess their validity and discuss systematic uncertainties not addressed so far.

A. Antiprotons

As we have stressed earlier, one of the main reasons why we could improve previous antiproton limits is the statistical analysis we have adopted. In particular, we took into account that nuclear uncertainties are not uncorrelated in energy (as was done, e.g., in Ref. [79]), while still allowing in our fits for the whole range of both nuclear and propagation uncertainties typically accounted for in the literature. Even though one might in principle still worry that these uncertainties may in reality be larger, in particular when considering more complicated propagation models, it is worthwhile to emphasize again that our simple three-parameter background model provides an extremely good fit to the data. Despite a certain degeneracy in these three parameters, in fact, the data constrain the shape of the background flux extremely tightly—which is the reason we can derive strong limits in particular for light DM contributions, which feature a somewhat different spectral shape of the antiproton flux at low energies (for a given value of the Fisk potential).

As demonstrated in Fig. 11, it is indeed almost the full data range that is responsible for setting the limits, not only the lowest data bins. Even though the DM contribution is negligible at higher energies, e.g., all data points below about 20 GeV contribute significantly to fixing *all* parameters $(\alpha_{\rm prop}, \alpha_{\rm nuc}, \phi_F)$. As a consequence, the DM contribution at these energies cannot easily be compensated by a change in those parameters. In fact, even neglecting data points below $T_{\bar{p}} \sim 1$ GeV in the analysis allows one to set

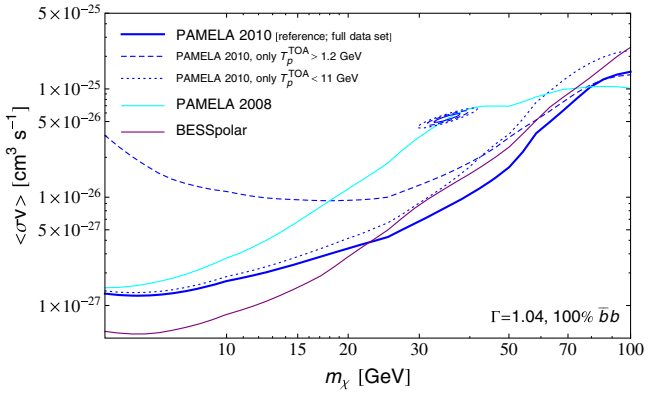

FIG. 11 (color online). Reference $\bar{p}$ limits and dependence on energy cuts and/or different data sets (assuming an NFW-like profile, with $\Gamma = 1.04$, and annihilation into $\bar{b}b$). For comparison, we also show the claimed signal region for a DM interpretation of the GC GeV excess in this channel [21].

stringent limits due to the very small error bars in the data at intermediate energies (unless, obviously, one considers very low DM masses).

In the same figure, we show for comparison also limits obtained with the older PAMELA data [82] and the data taken by the BESS-Polar experiment [158]. Interestingly, the updated PAMELA analysis allows one to place significantly stronger limits on a DM contribution exactly in the range of masses relevant for the GC GeV excess (in particular for the $\bar{b}b$ channel; for lighter quarks the difference is less pronounced). Notably, this is not mainly due to the longer observation time but due to an optimized "spillover" analysis [82] that results in a somewhat different shape of the best-fit background model: In contrast to the old data, the new PAMELA data [82] favor the maximal possible flux contribution that can be attributed to nuclear and propagation uncertainties (i.e., $\alpha_{\rm prop} = \alpha_{\rm nuc} = 1$), which is compensated by a significantly larger best-fit value for the Fisk potential ϕ_F (769 MV rather than 496 MV). Despite smaller error bars, this improves the total χ^2 of the best-fit model by more than 2. In view of these relatively large differences, it is comforting to see that an analysis of the BESS-Polar data results in limits that are comparable to the ones obtained with the newer PAMELA data.[7]

Another potential systematic limitation of our analysis is our treatment of solar modulation. The full four-dimensional propagation equations, including the diffusion and drift motion along the large scale gradients of the spiraling

[7]BESS-Polar only measured antiproton energies up to 4.7 GeV, which limits the possibility to constrain large DM masses if the Fisk potential is left as a completely unconstrained parameter in the analysis. We thus imposed the very conservative [159] restriction of $\phi_F < 1.5$ GV in our fits, which starts to affect limits from BESS-Polar for $m_\chi \gtrsim 30$ GeV, but has no effect on any of the other limits shown in Fig. 11 or elsewhere.

solar magnetic field, the heliospheric current sheet, and the radially expanding solar wind, were recently implemented in the numerical code HELIOPROP [160]. Reference [79] employed this code to analyze in detail the effect of solar modulation on cosmic-ray antiprotons from DM annihilation. On the other hand, a well-known analytic solution to the effect of the heliosphere on the flux of cosmic rays—the *force-field approximation* [80,81]—is obtained under the simplifying assumption of spherical symmetry and constant diffusion. It relates the LIS to the TOA flux with a single modulation parameter, the Fisk potential ϕ_F, via (see Refs. [161,162] for a derivation and discussion)

$$\frac{\Phi_{\rm TOA}(T_{\rm TOA})}{\Phi_{\rm LIS}(T_{\rm LIS})} = \frac{p^2_{\rm TOA}}{p^2_{\rm LIS}} = \frac{T_{\rm TOA}(T_{\rm TOA}+2m_p)}{T_{\rm LIS}(T_{\rm LIS}+2m_p)}, \quad (8)$$

with kinetic energies related by $T_{\rm TOA} = T_{\rm LIS} - \phi_F$.

In Fig. 12, we compare the numerical results from Ref. [79] that were obtained with HELIOPROP for two specific sets of propagation parameters with the results that we find by simply applying the force-field approximation, Eq. (8), as we did in our analysis. As benchmark scenarios we adopt one of the channels that well reproduce the gamma-ray GeV excess, $\chi\chi \to \bar{b}b$ with $m_\chi = 30$ GeV, assuming a thermal annihilation cross section, and the MED and MAX scenarios [85] for the antiproton propagation in the Galaxy. We find that, when adopting a Fisk potential of $\phi_F = 500$ MeV, the force-field approximation reproduces the numerical results remarkably well. Though a detailed comparison between the force-field approximation and a large set of heliospheric propagation parameters

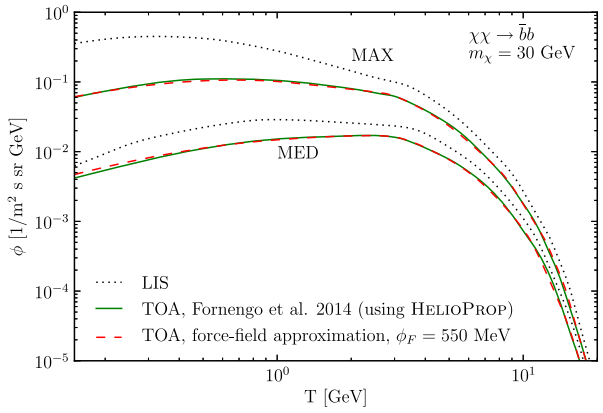

FIG. 12 (color online). Comparison of the force-field approximation to solar modulation with numerical results using HELIOPROP [160]. The dotted black line shows the local interstellar flux as a function of the antiproton kinetic energy; the dashed and solid lines show the top-of-atmosphere flux obtained from the force-field approximation and the numerical results from Ref. [79]. We adopt here as two exemplary LIS fluxes the antiproton signals from $\chi\chi \to \bar{b}b$ with a thermal cross section, $m_\chi = 30$ GeV, and using the MED and MAX cosmic-ray propagation scenarios [85], respectively.

is still lacking, we conclude that the force-field approximation is very well suited to study the impact of solar modulation on DM searches with antiprotons for kinetic energies $T_{\bar{p}} \gtrsim 0.1$ GeV. In particular, uncertainties related to heliospheric propagation appear negligible with respect to uncertainties coming from cosmic-ray propagation in the Galaxy.

Finally, let us remark that in the above analysis, we followed the common approach of adding statistical and systematic error bars in quadrature to obtain an estimate for the overall flux uncertainty. This step neglects possible bin-to-bin correlations between the systematic errors, which in the case of the PAMELA data may be overly optimistic [84]. A correct treatment of systematic uncertainties would require knowledge about the covariance matrix of the systematic errors, which is, however, not available. The impact on our results would then, in principle, critically depend on the spectral similarity between the principal components of the covariance matrix and the shape of signal and background fluxes.

While we leave a more detailed study to future work, let us here briefly illustrate the possible impact of correlated systematical errors on our results for a few simple toy scenarios. First, we allow the *normalization* of the measured flux to vary by $\pm 5\%$, corresponding to the typical error stated for the PAMELA 2010 data. We implement this in the fit as a constrained rescaling factor, $\alpha_s \in [0.95, 1.05]$, for the measured fluxes. Second, we allow the *spectral index* of the measured flux to vary. This is implemented as an energy-dependent prefactor $\alpha_t(E) = 1 + \kappa \log(E/\sqrt{E_{\rm mn}E_{\rm min}})$, where $|\kappa| \leq 0.05/\log(E_{\rm max}/E_{\rm min})$. The logic here is that the *maximal* deviation that we obtain at the end points of the measured spectrum deviates by up to 5% from the nominal value. Accounting for correlated systematics in this way, we find that our limits would be weakened by barely more than a factor of 2, thus not affecting our conclusions for the reference propagation model.

B. Positron limits

Systematic uncertainties that play a role when constraining DM annihilation into leptonic final states with the positron flux measurements of AMS-02 were discussed in detail in Ref. [104]. Here, we briefly summarize the main aspects.

The propagation of cosmic-ray electrons (and positrons) is dominated by energy losses rather than by diffusion, namely by efficient synchrotron radiation on the Galactic magnetic field and by inverse Compton scattering on starlight, thermal dust radiation, and the CMB. As a consequence, positrons are a much more local probe of DM annihilation than the other messengers that we have considered here. In the case of the channel that is most constrained by AMS-02 data, annihilation into electron-positron pairs, the resulting spectrum after propagation has a sharp steplike cutoff at energies $E_{e^\pm} = m_\chi$, with a long

tail toward lower energies. The electron flux at this energy, and hence the height of the step, depends almost exclusively on the local energy-loss rate, and hence on the local radiation field, which can be estimated to within 50%. The details of the propagation scenario (height of diffusive halo, etc.) play, on the other hand, only a marginal role for the steplike signal.

Solar modulation will affect the TOA flux of cosmic-ray electrons at energies below 5–10 GeV. For DM masses around $m_\chi \approx 10$ GeV, this is not relevant for e^+e^- and $\mu^+\mu^-$ final states, where the relevant peak of the signal is close to the DM mass, but it can slightly affect limits in case of the broader $\tau^+\tau^-$ spectrum.

Last, the discreteness of astrophysical sources that might cause the rise in the positron fraction can potentially lead to small variations in the measured energy spectrum. This is currently not observed, but can lead to a variation of the limits on e^+e^- final states by up to a factor of about 3.

C. Radio limits

Our limits in the radio band are essentially based on three main assumptions: (i) diffusion, advection effects and energy losses other than those due to synchrotron emission can be neglected, (ii) energy equipartition in the accretion zone, i.e., at galactocentric distances smaller than $\sim$0.04 pc, and magnetic flux conservation outside, (iii) the monochromatic approximation for synchrotron emission. As already discussed, however, a strong magnetic field as adopted in our model is observationally well supported [119], and our limits are rather insensitive to the monochromatic approximation; we will hence mostly concentrate on a discussion of (i).

In deriving Eq. (5) as a condition for (i) to be satisfied, we made use of the fact that for sufficiently large magnetic fields and turbulent conditions the diffusion coefficient approaches the critical (i.e., minimum possible) value of $D \sim D_{\rm Bohm} = r_g c/3$. Deviations from the assumption of Bohm diffusion will lead to less frequent scattering and more efficient transport, $D = \kappa D_{\rm Bohm}$, where we introduced a free parameter $\kappa \geq 1$ to account for this possibility. Importantly, even allowing $\kappa \gg 1$ the condition for the neglect of diffusion in Eq. (5) scales only with a factor of $\kappa^{1/3}$ on the right-hand side (at least for constant B). This has profound consequences for the robustness of our radio limits: The bulk of the radio signal of interest comes from a relatively small range of distances from the Galactic center, around $r \sim 0.1$ pc, depending on the shape of the DM profile (see Fig. 8). Observations give a lower limit on the magnetic field that is around 8 mG [119] at these scales. We thus find that at $r \simeq 0.1$ pc diffusion can be neglected even if the diffusion constant is $\sim 10^7$ times larger than the Bohm value.

Since the requirement of *in situ* energy loss is very well satisfied, our limits depend much more on the DM profile than on the magnetic field strength. This is visualized in Fig. 9, but also directly apparent from Eq. (6) where ρ_χ enters squared and gives a particularly large contribution to the volume integration for singular profiles. The product $EN_e(E)$, on the other hand, determines the dependence on B (implying in fact slightly stronger limits for weaker magnetic fields). In the limit of $E \ll m_\chi$, corresponding to large magnetic field values, $N_e(E)$ approaches a constant and the synchrotron flux scales as $E \propto B^{-1/2}$. In general, $N_e(E)$ is a monotonically decreasing function of E, which implies that the actual B dependence of Eq. (6) will in practice be smaller. An intuitive way to understand this relatively weak dependence of the flux density for a given frequency is that, in the limit of synchrotron losses happening *in situ* as discussed above, the value of B does not affect anymore the total power radiated away but merely the frequency at which this happens. Note also that for larger magnetic fields B, we do not need to follow the superconservative approach of only integrating up to 1 pc (see Fig. 8). This implies that—in case of cored profiles—limits will realistically weaken even less with increased magnetic field values.

To illustrate the scaling of the limits with B, we present in Fig. 13 the cases where the magnetic field takes the constant values $B = 50\ \mu$G and $B = 8$ mG, as motivated by the recently obtained lower limits [119] discussed above, and compare the resulting limits with those shown for our baseline magnetic field model in Fig. 10. Interestingly, the case of a constant magnetic field of $B = 50\ \mu$G leads indeed to very similar limits. At DM masses $m_\chi \gg 50$ GeV, limits *weaken* as expected with a factor of $(8\ \text{mG}/50\ \mu\text{G})^{1/2} \sim 13$ when instead adopting the much larger constant field of $B = 8$ mG. At low masses, they may, however, even *strengthen* due to the $N_e(E)$ dependence discussed above. In both cases, we see that DM annihilation into $80\%80\%\tau^+\tau^- + 20\%\bar{b}b$ leads to limits that exclude the interpretation of the excess in terms of such

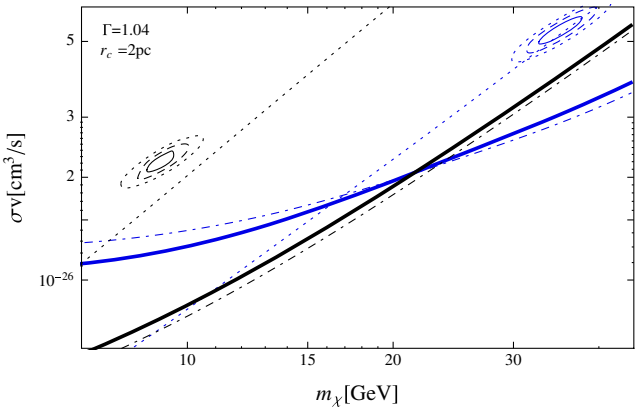

FIG. 13 (color online). Same as Fig. 9, but for constant magnetic fields of strength $B = 50\ \mu$G (dot-dashed lines), $B = 8$ mG (dotted lines), and our baseline magnetic field model (solid lines). The constant values correspond to the recently obtained lower limits at a galactocentric distance of $\sim$0.1 pc [119].

annihilations, whereas a large magnetic field of $B = 8$ mG would require a slightly smaller core size in the profile, $r_c \lesssim 2$ pc, to fully exclude also the possibility of $\bar{b}b$ final states.

Let us conclude this section by mentioning a very recent analysis [163] that revisited radio constraints on DM annihilation in the GC. In particular, this analysis challenges the standard assumption of *in situ* energy losses of the emitted electrons due to synchrotron radiation when taking into account inverse Compton scattering (ICS), or strong convective winds in the inner Galaxy. For the magnetic field model that we have adopted, e.g., the limits are claimed to weaken by more than 2 orders of magnitude when including ICS off the dense interstellar radiation field close to the GC (but note that the actual B field is likely stronger, as discussed above, which would make ICS less important in proportion). Together with the assumption of a very strong convective wind that blows electrons away from the galactic disk with a velocity of $v_c \sim 1000$ km/s, this would result in a weakening of our limits by less than 4 orders of magnitude in total. For a steep profile with $\Gamma = 1.26$, however, even this extreme case is not sufficient to make the GC excess compatible with radio observations unless one introduces an artificial cutoff at $r_c \gtrsim 0.1$ pc.

V. SUMMARY

In Fig. 14 we present a summary of the constraints on DM annihilation that we derived from antiproton, positron, and radio observations, and confront them with representative benchmark scenarios that can explain the GC GeV excess observed with Fermi-LAT. Since the annihilation cross section that best reproduces the gamma-ray signal depends on the assumption on the DM profile, in particular the inner slope Γ and the local DM density, in Fig. 14 we normalize the annihilation cross section to the values that best reproduce the GeV excess (cf. Table I). In this way, we collapse the best-fit regions into one single region, which is per construction centered onto one. The limits change then according to the slope Γ (and the scale radius r_s, which we will comment on below), whereas the overall normalization of the DM profile drops out (as do symmetry factors in the annihilation rate related to whether the DM particles are their own antiparticles).

In the case of DM annihilation into $\bar{b}b$ final states, as shown in the upper left panel of Fig. 14, limits from existing observations of antiprotons firmly exclude the DM interpretation of the GeV excess by almost 1 order of magnitude, if our benchmark KRA scenario is adopted for the propagation of Galactic cosmic rays. These limits weaken by about a factor of 2 if Γ increases from $\Gamma = 1.04$ to $\Gamma = 1.26$. Note that, as shown in Fig. 1, variations in the scale radius r_s introduce another uncertainty in the *local* annihilation rate that can be as large as a factor of 2, which in case of very cuspy profiles (like $\Gamma = 1.26$) will typically tend to *increase* the annihilation signal when mass constraints on the Milky Way are taken into account. However, we checked explicitly that the antiproton limits—which probe a relatively large annihilation volume—are only strengthened by 24% (weakened by 39%) when changing our references value of r_s from 20 kpc to 35 kpc (10 kpc). As shown in Fig. 5, in the case of the very conservative MIN' propagation scenario the limits can weaken by an additional factor of 7–8. Only in this extreme propagation setting would the GeV excess still be marginally consistent with current antiproton observations—implying that AMS-02 will either observe a corresponding excess in antiprotons or rule out even this remaining possibility.

We also show limits obtained from 408 MHz Jodrell Bank radio observations of the inner 4" centered on the GC. As discussed above, these limits are rather robust concerning assumptions on the magnetic field, but they critically depend on the adopted DM profile. Most importantly, in the case of the gamma-ray excess, the DM profile is fixed to a large extent, allowing one to make much more precise signal predictions. For a profile that remains cuspy all the way down to $\lesssim$0.1 pc, all channels that could explain the GeV excess are ruled out by several orders of magnitude (cf. Fig. 9)—though these limits become much less severe when allowing for strong convective winds or ICS to dominate over synchrotron emission [163]. In Fig. 14, we show limits that are obtained for an *ad hoc* flattening of the generalized NFW profile at radii below 2 pc. Even with such an artificial core, in case of the cuspy $\Gamma = 1.26$ the limits still exclude the DM interpretation of the GeV excess by more than 1 order of magnitude. Note that GC radio observations only probe the innermost region of the DM halo. The resulting limits thus do not depend on the scale radius r_s; see Fig. 1. For the same reason, steeper profiles imply much *stronger* radio constraints in the context of the GeV excess, while they imply slightly *weaker* constraints for antiprotons. In the case of DM annihilation into $\bar{c}c$ or light quarks $\bar{q}q$ (upper right and lower left panel of Fig. 14), the limits obtained from radio and antiproton observations are quantitatively very similar to the case of $\bar{b}b$.

In the lower right panel of Fig. 14, we finally show limits on the mixed final state $\tau^+\tau^-$ (80%) plus $\bar{b}b$ (20%), which was motivated in Ref. [21] by a spectral fit to the excess seen in the inner Galaxy (see also the discussion in Sec. II A). In this case, antiproton constraints only lead to an exclusion by a factor of roughly 2 in the case of the KRA propagation scenario (and no exclusion if the MIN' model is adopted). However, radio limits firmly exclude this channel for a DM profile that remains cuspy down to at least 2 pc. Additional robust constraints derive from the shape analysis [104] of the flux of cosmic-ray positrons as measured by AMS-02, which again marginally excludes the interpretation of the gamma-ray GeV excess in terms of DM annihilation into $\tau^+\tau^-$ final states for a cuspy profile with $\Gamma = 1.26$ (as preferred by the inner galaxy analysis of Ref. [21]). As discussed above (see Figs. 6 and 7), these

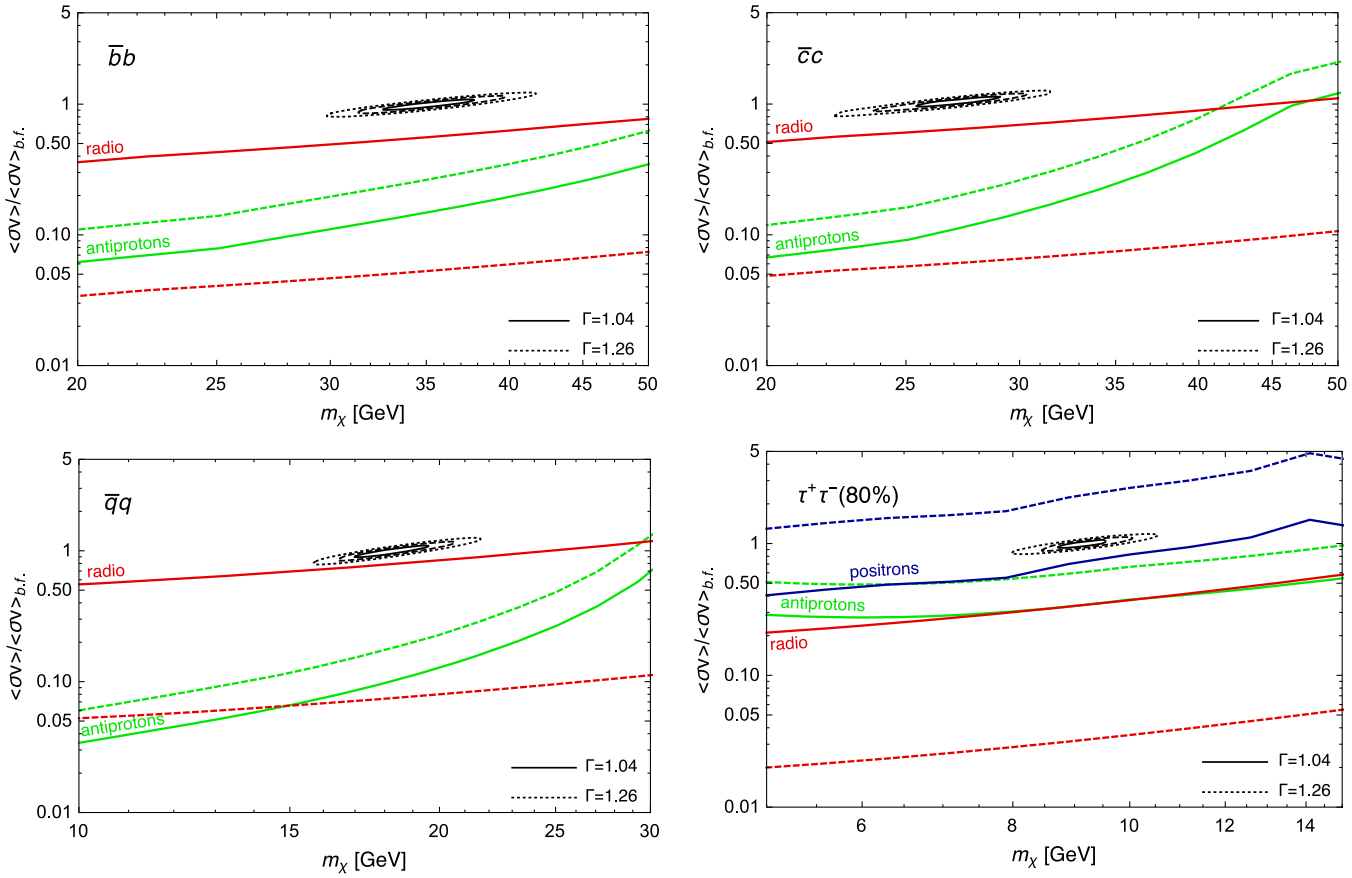

FIG. 14 (color online). *Summary of our limits* for various annihilation channels, expressed in terms of the *ratio* of the corresponding limit on $\langle\sigma v\rangle$ and the best-fit DM signal interpretation. For convenience, we also show the corresponding 1σ, 2σ, and 3σ regions describing the signal from the inner Galaxy analysis [21] (see also Fig. 2). Dashed lines show limits for a generalized NFW profile with slope $\Gamma = 1.26$ and solid lines show the corresponding limits for $\Gamma = 1.04$ (note that the limits presented this way are independent of any overall normalization of the DM profile, e.g., in terms of the local DM density $\rho_\odot = 0.3$ GeV cm^{-3}). In all panels, antiproton limits are displayed in green, positron limits in blue, and radio limits in red. Radio constraints assume that the DM profile flattens out at radii below 2 pc from the GC. See text for further details.

limits are *much* stronger in case of other leptonic final states, and exclude branching ratios into e^+e^- down to about $\sim 2.3 \times 10^{-2}$, and down to $\sim 2.5 \times 10^{-1}$ in the case of $\mu^+\mu^-$ final states. Note that uncertainties related to the scale radius r_s of the DM profile are larger than for antiprotons and can in principle be as large as a factor of 2; for $\Gamma = 1.26$, however, they tend to *increase* the local annihilation signal.

We recall that a larger contribution of $\tau\tau$ final states than 80% results in a spectrum that no longer provides a reasonable fit to the observed GeV excess, even when taking into account the contribution from bremsstrahlung and inverse Compton scattering. A smaller contribution, on the other hand, necessarily implies a larger $\bar{b}b$ (or lighter quark) contribution in view of the strong AMS-02 limits on light leptons as annihilation products. While a mixed final state with a smaller $\tau^\pm$ component could evade AMS-02 bounds, the antiproton bounds from PAMELA would thus become even more severe.

In summary, we find that the DM interpretation of the GeV excess in terms of hadronic or leptonic final states is strongly constrained by our analysis of existing antiproton, positron, and radio data. A way to make these limits even more robust would be to study diffusion parameters, in particular the truly minimal diffusion zone height, in light of existing radio, gamma-ray, and cosmic-ray observations in a *combined* analysis. For the case of antiproton limits, the most important next step would then be to systematically improve on the nuclear uncertainties connected to secondary antiproton production. For positron limits on $\tau^+\tau^-$ final states, on the other hand, a dedicated study of the effects of solar modulation on the spectrum of DM induced positrons below energies of $\sim$5 GeV would be more warranted. Avoiding the radio limits we have presented requires a dedicated discussion of what mechanisms could give rise to a DM profile that is cuspy in the inner Galaxy, down to $\mathcal{O}(10)$ pc scales, but has a core with an extension of a few pc at its center. Last but not least, it will certainly

help to get a better handle on the systematics connected to the determination of the DM profile slope Γ, as well as the scale radius r_s, from gamma-ray and dynamical observations.

While all those possible directions of further investigation clearly lie beyond the scope of the present study, they certainly indicate that there is room to make indirect DM searches even more competitive—especially for light DM models, but independently of the concrete application of the GeV gamma-ray excess currently claimed at the GC and inner Galaxy.

VI. CONCLUSIONS

In this article, we have revisited current bounds from indirect searches for DM and identified the messengers and targets that are most relevant for light DM, i.e., for masses roughly below 100 GeV:

(i) For DM annihilation into light charged leptons, *positrons* provide the most stringent and robust bounds [104,105]. This constrains the "thermal" annihilation rate of $\langle\sigma v\rangle = 3 \times 10^{-26}$ cm^3 s^{-1} for masses of roughly $m_\chi \lesssim 200$ GeV ($m_\chi \lesssim 100$ GeV) assuming dominant annihilation to e^+e^- ($\mu^+\mu^-$) final states.

(ii) As has been pointed out earlier, *antiprotons* provide a very efficient means of constraining light DM annihilating into quarks [95,164–166]. Here, we have derived new bounds that constrain the thermal annihilation rate for $m_\chi \lesssim 55$ GeV in the case of $\bar{b}b$ final states, and for $m_\chi \lesssim 35$ GeV if annihilation into light quarks dominates.

(iii) Null searches for 408 MHz *radio signals* from a 4" region around the GC, finally, provide extremely stringent constraints [107–115]. We revisited those bounds and discussed that the dependence on assumptions about the magnetic field is typically much smaller than that related to the DM density at pc scales away from the GC. For a cuspy profile (like NFW) that extends down to at least 0.1 pc, thermal cross sections are excluded for DM masses below roughly 120 GeV (for $\tau^+\tau^-$) or even 400 GeV (for $\bar{b}b$).

As an application, we have discussed at length that these findings are particularly relevant for a possible DM interpretation of the much-debated excess in GeV gamma rays from the GC and inner Galaxy [21–27]. In fact, such an interpretation requires a well-defined and highly constrained region both in the $\langle\sigma v\rangle$ vs m_χ plane and in the range of possible DM density profiles. This implies that constraints from other indirect detection methods can directly be applied and are subject to much less severe uncertainties than in the absence of a signal indication. For example, these constraints become independent of the overall normalization of the annihilation rate and thus, e.g., of the DM production mechanism. In fact, probing the same annihilation mechanism, such constraints are much more model-independent than constraints derived from collider or direct searches [43–47].

For reasonable benchmark scenarios for cosmic-ray propagation and a DM density profile consistent with the observed excess, we basically find that all annihilation channels that were considered in Ref. [21] are ruled out (the same holds for purely leptonic annihilation channels, which were suggested in Ref. [62]). The tension can be somewhat alleviated by (a) assuming a borderline propagation scenario with minimal diffusion zone height (our MIN') *and* (b) assuming that the DM profile cuts off at radii of at least $\sim$5 pc from the Galactic center (while keeping its $\Gamma = 1.26$ slope observed at larger radii $r \gtrsim 10$ pc). On the model-building side, the tension could also be made somewhat less severe by considering cascade decays [36,39,167] rather than the direct decay into two SM particle final states that we have considered here. While a thorough investigation of this possibility lies beyond the scope of this work, we do not expect our conclusions to change qualitatively.

A confirmation of the DM interpretation of the GeV excess clearly requires corroborating evidence from multiple observations. While this could also come from collider or direct probes, indirect searches arguably provide the most model-independent way of testing the signal. Even though the excess is already in rather strong tension with these searches, it is conceivable that the individual uncertainties of the respective limits (as discussed in Sec. IV and summarized in Sec. V) conspire such that a signal interpretation would still be viable. In this case, an independent confirmation of the GeV excess as a DM signal—if indeed true—is likely to be just around the corner.

ACKNOWLEDGMENTS

We would like to thank Lars Bergström, Celine Boehm, Mirko Boezio, Carmelo Evoli, Dan Hooper, Tim Linden, Meng Su, Jacco Vink, and Wei Xue for very useful discussions. T. B. acknowledges support from the German Research Foundation (DFG) through the Emmy Noether Grant No. BR 3954/1-1. T. B. and C. W. thank NORDITA for generous support and an inspiring atmosphere in the context of the programme "What is Dark Matter?" where part of this work was completed. M. V. acknowledges support from the Forschungs- und Wissenschaftsstiftung Hamburg through the program "Astroparticle Physics with Multiple Messengers." This work makes use of SciPy [168], Minuit [169], and Matplotlib [170].

Note added.—After the submission of this work, another comprehensive analysis of antiproton constraints on the GeV excess appeared on the arXiv [171], adopting a somewhat different background parameterization and statistical method.

[1] M. Cirelli, Pramana **79**, 1021 (2012).
[2] J. Lavalle and P. Salati, C. R. Phys. **13**, 740 (2012).
[3] T. Bringmann and C. Weniger, Phys. Dark Univ. **1**, 194 (2012).
[4] A. Cesarini, F. Fucito, A. Lionetto, A. Morselli, and P. Ullio, Astropart. Phys. **21**, 267 (2004).
[5] D. Horns, Phys. Lett. B **607**, 225 (2005); **611**, 297(E) (2005).
[6] L. Bergstrom, T. Bringmann, M. Eriksson, and M. Gustafsson, Phys. Rev. Lett. **94**, 131301 (2005).
[7] T. Bringmann, X. Huang, A. Ibarra, S. Vogl, and C. Weniger, J. Cosmol. Astropart. Phys. 07 (2012) 054.
[8] C. Weniger, J. Cosmol. Astropart. Phys. 08 (2012) 007.
[9] M. Su and D. P. Finkbeiner, arXiv:1206.1616.
[10] A. V. Belikov, G. Zaharijas, and J. Silk, Phys. Rev. D **86**, 083516 (2012).
[11] D. Hooper, D. P. Finkbeiner, and G. Dobler, Phys. Rev. D **76**, 083012 (2007).
[12] C. Boehm, D. Hooper, J. Silk, M. Casse, and J. Paul, Phys. Rev. Lett. **92**, 101301 (2004).
[13] L. Bergstrom, P. Ullio, and J. H. Buckley, Astropart. Phys. **9**, 137 (1998).
[14] T. Bringmann, F. Calore, G. Vertongen, and C. Weniger, Phys. Rev. D **84**, 103525 (2011).
[15] R. E. Lingenfelter, J. C. Higdon, and R. E. Rothschild, Phys. Rev. Lett. **103**, 031301 (2009).
[16] D. T. Cumberbatch, J. Zuntz, H. K. K. Eriksen, and J. Silk, arXiv:0902.0039.
[17] F. Aharonian *et al.* (H.E.S.S. Collaboration), Phys. Rev. Lett. **97**, 221102 (2006); **97**, 249901(E) (2006).
[18] F. W. Stecker, S. D. Hunter, and D. A. Kniffen, Astropart. Phys. **29**, 25 (2008).
[19] M. Ackermann *et al.* (Fermi-LAT Collaboration), Phys. Rev. D **88**, 082002 (2013).
[20] See http://fermi.gsfc.nasa.gov/ssc/.
[21] T. Daylan, D. P. Finkbeiner, D. Hooper, T. Linden, S. K. N. Portillo, N. L. Rodd, and T. R. Slatyer, arXiv:1402.6703.
[22] L. Goodenough and D. Hooper, arXiv:0910.2998.
[23] D. Hooper and L. Goodenough, Phys. Lett. B **697**, 412 (2011).
[24] D. Hooper and T. Linden, Phys. Rev. D **84**, 123005 (2011).
[25] K. N. Abazajian and M. Kaplinghat, Phys. Rev. D **86**, 083511 (2012).
[26] O. Macias and C. Gordon, Phys. Rev. D **89**, 063515 (2014).
[27] K. N. Abazajian, N. Canac, S. Horiuchi, and M. Kaplinghat, Phys. Rev. D **90**, 023526 (2014).
[28] D. Hooper and T. R. Slatyer, Phys. Dark Univ. **2**, 118 (2013).
[29] W.-C. Huang, A. Urbano, and W. Xue, arXiv:1307.6862.
[30] D. Hooper, Phys. Dark Univ. **1**, 1 (2012).
[31] A. Hektor and L. Marzola, Phys. Rev. D **90**, 053007 (2014).
[32] P. Agrawal, B. Batell, D. Hooper, and T. Lin, Phys. Rev. D **90**, 063512 (2014).
[33] D. G. Cerdeño, M. Peiró, and S. Robles, J. Cosmol. Astropart. Phys. 08 (2014) 005.
[34] S. Ipek, D. McKeen, and A. E. Nelson, Phys. Rev. D **90**, 055021 (2014).
[35] P. Ko, W.-I. Park, and Y. Tang, J. Cosmol. Astropart. Phys. 09 (2014) 013.
[36] C. Boehm, M. J. Dolan, and C. McCabe, Phys. Rev. D **90**, 023531 (2014).
[37] M. Abdullah, A. DiFranzo, A. Rajaraman, T. M. P. Tait, P. Tanedo, and A. M. Wijangco, Phys. Rev. D **90**, 035004 (2014).
[38] D. K. Ghosh, S. Mondal, and I. Saha, arXiv:1405.0206.
[39] A. Martin, J. Shelton, and J. Unwin, arXiv:1405.0272 [Phys. Rev. D (to be published)].
[40] A. Berlin, P. Gratia, D. Hooper, and S. D. McDermott, Phys. Rev. D **90**, 015032 (2014).
[41] T. Basak and T. Mondal, arXiv:1405.4877.
[42] J. M. Cline, G. Dupuis, Z. Liu, and W. Xue, J. High Energy Phys. 08 (2014) 131.
[43] A. Alves, S. Profumo, F. S. Queiroz, and W. Shepherd, arXiv:1403.5027.
[44] A. Berlin, D. Hooper, and S. D. McDermott, Phys. Rev. D **89**, 115022 (2014).
[45] E. Izaguirre, G. Krnjaic, and B. Shuve, Phys. Rev. D **90**, 055002 (2014).
[46] K. Kong and J.-C. Park, Nucl. Phys. **B888**, 154 (2014).
[47] T. Han, Z. Liu, and S. Su, J. High Energy Phys. 08 (2014) 093.
[48] F. Calore, I. Cholis, and C. Weniger, arXiv:1409.0042.
[49] K. N. Abazajian, J. Cosmol. Astropart. Phys. 03 (2011) 010.
[50] W. Wang, Z. J. Jiang, and K. S. Cheng, Mon. Not. R. Astron. Soc. **358**, 263 (2005).
[51] A. Boyarsky, D. Malyshev, and O. Ruchayskiy, Phys. Lett. B **705**, 165 (2011).
[52] F. Yusef-Zadeha *et al.*, Astrophys. J. **762**, 33 (2013).
[53] T. Linden, E. Lovegrove, and S. Profumo, Astrophys. J. **753**, 41 (2012).
[54] C. Gordon and O. Macias, Phys. Rev. D **88**, 083521 (2013).
[55] S. K. N. Portillo and D. P. Finkbeiner, arXiv:1406.0507 [Astrophys. J. (to be published)].
[56] O. Y. Gnedin, A. V. Kravtsov, A. A. Klypin, and D. Nagai, Astrophys. J. **616**, 16 (2004).
[57] J. F. Navarro, C. S. Frenk, and S. D. M. White, Astrophys. J. **462**, 563 (1996).
[58] F. Iocco, M. Pato, G. Bertone, and P. Jetzer, J. Cosmol. Astropart. Phys. 11 (2011) 029.
[59] L. Pieri, J. Lavalle, G. Bertone, and E. Branchini, Phys. Rev. D **83**, 023518 (2011).
[60] M. Cirelli, G. Corcella, A. Hektor, G. Hutsi, M. Kadastik, P. Panci, M. Raidal, F. Sala, and A. Strumia, J. Cosmol. Astropart. Phys. 03 (2011) 051; 10 (2012) E01.
[61] X. X. Xue *et al.* (SDSS Collaboration), Astrophys. J. **684**, 1143 (2008).
[62] T. Lacroix, C. Boehm, and J. Silk, Phys. Rev. D **90**, 043508 (2014).
[63] A. A. Abdo *et al.* (The Fermi-LAT Collaboration), Astrophys. J. Suppl. Ser. **208**, 17 (2013).
[64] D. Hooper, I. Cholis, T. Linden, J. Siegal-Gaskins, and T. Slatyer, Phys. Rev. D **88**, 083009 (2013).
[65] F. Calore, M. Di Mauro, and F. Donato, Astrophys. J. **796**, **1**, 14 (2014).
[66] Q. Yuan and B. Zhang, J. High Energy Astrophys. **3–4**, 1 (2014).

[67] F. Aharonian *et al.* (H.E.S.S. Collaboration), Nature (London) **439**, 695 (2006).
[68] J. Petrovic, P. D. Serpico, and G. Zaharijas, J. Cosmol. Astropart. Phys. 10 (2014) 052.
[69] E. Carlson and S. Profumo, Phys. Rev. D **90**, 023015 (2014).
[70] P. Gondolo, J. Edsjö, P. Ullio, L. Bergström, M. Schelke, E. A. Baltz, T. Bringmann, and G. Duda, http://www.darksusy.org; P. Gondolo, J. Edsjo, P. Ullio, L. Bergstrom, M. Schelke, and E. A. Baltz, J. Cosmol. Astropart. Phys. 07 (2004) 008.
[71] T. Sjostrand, S. Mrenna, and P. Z. Skands, J. High Energy Phys. 05 (2006) 026.
[72] J. Silk and M. Srednicki, Phys. Rev. Lett. **53**, 624 (1984).
[73] For a review see, e.g., P. Salati, F. Donato, and N. Fornengo, in *Particle Dark Matter: Observations, Models and Searches*, edited by G. Bertone (Cambridge University Press, Cambridge, UK, 2010), pp. 521–546.
[74] T. Bringmann and P. Salati, Phys. Rev. D **75**, 083006 (2007).
[75] F. Donato, D. Maurin, P. Salati, A. Barrau, G. Boudoul, and R. Taillet, Astrophys. J. **563**, 172 (2001).
[76] D. Maurin, F. Donato, R. Taillet, and P. Salati, Astrophys. J. **555**, 585 (2001).
[77] M. di Mauro, F. Donato, A. Goudelis, and P. D. Serpico, Phys. Rev. D **90**, 085017 (2014).
[78] R. Kappl and M. W. Winkler, J. Cosmol. Astropart. Phys. 09 (2014) 051.
[79] N. Fornengo, L. Maccione, and A. Vittino, J. Cosmol. Astropart. Phys. 04 (2014) 003.
[80] L. J. Gleeson and W. I. Axford, Astrophys. J. **154**, 1011 (1968).
[81] J. S. Perko, Astron. Astrophys. **184**, 119 (1987).
[82] O. Adriani *et al.*, Pis'ma Zh. Eksp. Teor. Fiz. **96**, 693 (2012) [JETP Lett. **96**, 621 (2013)].
[83] O. Adriani *et al.* (PAMELA Collaboration), Phys. Rev. Lett. **105**, 121101 (2010).
[84] M. Boezio (private communication).
[85] F. Donato, N. Fornengo, D. Maurin, and P. Salati, Phys. Rev. D **69**, 063501 (2004).
[86] G. Di Bernardo, C. Evoli, D. Gaggero, D. Grasso, and L. Maccione, Astropart. Phys. **34**, 274 (2010).
[87] A. Putze, L. Derome, and D. Maurin, Astron. Astrophys. **516**, A66 (2010).
[88] T. Delahaye, A. Fiasson, M. Pohl, and P. Salati, Astron. Astrophys. **531**, A37 (2011).
[89] Fermi-LAT Collaboration, Astrophys. J. **750**, 3 (2012).
[90] T. Delahaye, F. Donato, N. Fornengo, J. Lavalle, R. Lineros, P. Salati, and R. Taillet, Astron. Astrophys. **501**, 821 (2009).
[91] J. Lavalle, Mon. Not. R. Astron. Soc. **414**, 985 (2011).
[92] T. Bringmann, F. Donato, and R. A. Lineros, J. Cosmol. Astropart. Phys. 01 (2012) 049.
[93] G. Di Bernardo, C. Evoli, D. Gaggero, D. Grasso, and L. Maccione, J. Cosmol. Astropart. Phys. 03 (2013) 036.
[94] J. Lavalle, D. Maurin, and A. Putze, Phys. Rev. D **90**, 081301 (2014).
[95] C. Evoli, I. Cholis, D. Grasso, L. Maccione, and P. Ullio, Phys. Rev. D **85**, 123511 (2012).
[96] L. Bergstrom, J. Edsjo, and P. Ullio, Astrophys. J. **526**, 215 (1999).
[97] W. A. Rolke, A. M. Lopez, and J. Conrad, Nucl. Instrum. Methods Phys. Res., Sect. A **551**, 493 (2005).
[98] R. Kappl and M. W. Winkler, Phys. Rev. D **85**, 123522 (2012).
[99] M. Cirelli and G. Giesen, J. Cosmol. Astropart. Phys. 04 (2013) 015.
[100] M. Tavakoli, I. Cholis, C. Evoli, and P. Ullio, J. Cosmol. Astropart. Phys. 01 (2014) 017.
[101] M. Aguilar *et al.* (AMS Collaboration), Phys. Rev. Lett. **110**, 141102 (2013).
[102] O. Adriani *et al.* (PAMELA Collaboration), Nature (London) **458**, 607 (2009).
[103] M. Ackermann *et al.* (Fermi-LAT Collaboration), Phys. Rev. Lett. **108**, 011103 (2012).
[104] L. Bergstrom, T. Bringmann, I. Cholis, D. Hooper, and C. Weniger, Phys. Rev. Lett. **111**, 171101 (2013).
[105] A. Ibarra, A. S. Lamperstorfer, and J. Silk, Phys. Rev. D **89**, 063539 (2014).
[106] R. D. Davies, D. Walsh, and R. S. Booth, Mon. Not. R. Astron. Soc. **177**, 319 (1976).
[107] P. Gondolo, Phys. Lett. B **494**, 181 (2000).
[108] G. Bertone, G. Sigl, and J. Silk, Mon. Not. R. Astron. Soc. **326**, 799 (2001).
[109] R. Aloisio, P. Blasi, and A. V. Olinto, J. Cosmol. Astropart. Phys. 05 (2004) 007.
[110] M. Regis and P. Ullio, Phys. Rev. D **78**, 043505 (2008).
[111] G. Bertone, M. Cirelli, A. Strumia, and M. Taoso, J. Cosmol. Astropart. Phys. 03 (2009) 009.
[112] T. Bringmann, arXiv:0911.1124.
[113] Y. Mambrini, M. H. G. Tytgat, G. Zaharijas, and B. Zaldivar, J. Cosmol. Astropart. Phys. 11 (2012) 038.
[114] R. Laha, K. C. Y. Ng, B. Dasgupta, and S. Horiuchi, Phys. Rev. D **87**, 043516 (2013).
[115] M. Asano, T. Bringmann, G. Sigl, and M. Vollmann, Phys. Rev. D **87**, 103509 (2013).
[116] F. Melia, Astrophys. J. **387**, L25 (1992).
[117] R. Beck and R. Wielebinski, in *Planets, Stars, and Stellar Systems*, edited by T. D. Oswalt and G. Gilmore (Springer, Dordrecht, 2013), Vol. 5, p. 978.
[118] C. Boehm, J. Silk, and T. Ensslin, arXiv:1008.5175.
[119] R. P. Eatough, Nature (London) **501**, 391 (2013).
[120] D. P. Marrone, J. M. Moran, J.-H. Zhao, and R. Rao, Astrophys. J. **654**, L57 (2007).
[121] V. F. Shvartsman, Sov. Astron. **15**, 377 (1971).
[122] S. L. Shapiro, Astrophys. J. **185**, 69 (1973).
[123] V. S. Berezinsky, A. V. Gurevich, and K. P. Zybin, Phys. Lett. B **294**, 221 (1992).
[124] P. Ullio, H. Zhao, and M. Kamionkowski, Phys. Rev. D **64**, 043504 (2001).
[125] D. Merritt, M. Milosavljevic, L. Verde, and R. Jimenez, Phys. Rev. Lett. **88**, 191301 (2002).
[126] S. Galli, F. Iocco, G. Bertone, and A. Melchiorri, Phys. Rev. D **80**, 023505 (2009).
[127] T. R. Slatyer, N. Padmanabhan, and D. P. Finkbeiner, Phys. Rev. D **80**, 043526 (2009).
[128] S. Galli, F. Iocco, G. Bertone, and A. Melchiorri, Phys. Rev. D **84**, 027302 (2011).
[129] T. R. Slatyer, Phys. Rev. D **87**, 123513 (2013).

[130] J. M. Cline and P. Scott, J. Cosmol. Astropart. Phys. 03 (2013) 044; 05 (2013) E01.
[131] L. Lopez-Honorez, O. Mena, S. Palomares-Ruiz, and A. C. Vincent, J. Cosmol. Astropart. Phys. 07 (2013) 046.
[132] J. Aleksić *et al.*, J. Cosmol. Astropart. Phys. 02 (2014) 008.
[133] M. Ackermann *et al.* (Fermi-LAT Collaboration), Phys. Rev. D **89**, 042001 (2014).
[134] I. Cholis and P. Salucci, Phys. Rev. D **86**, 023528 (2012).
[135] E. Aliu *et al.* (VERITAS Collaboration), Phys. Rev. D **85**, 062001 (2012).
[136] A. Geringer-Sameth and S. M. Koushiappas, Phys. Rev. Lett. **107**, 241303 (2011).
[137] A. Abramowski *et al.* (HESS Collaboration), Astropart. Phys. **34**, 608 (2011).
[138] A. A. Abdo *et al.* (Fermi-LAT Collaboration), Astrophys. J. **712**, 147 (2010).
[139] S. Ando and D. Nagai, J. Cosmol. Astropart. Phys. 07 (2012) 017.
[140] S. Zimmer *et al.* (Fermi-LAT Collaboration), arXiv: 1110.6863.
[141] X. Huang, G. Vertongen, and C. Weniger, J. Cosmol. Astropart. Phys. 01 (2012) 042.
[142] M. Ackermann *et al.*, J. Cosmol. Astropart. Phys. 05 (2010) 025.
[143] T. Bringmann, F. Calore, M. Di Mauro, and F. Donato, Phys. Rev. D **89**, 023012 (2014).
[144] A. A. Abdo *et al.* (Fermi-LAT Collaboration), J. Cosmol. Astropart. Phys. 04 (2010) 014.
[145] M. Shirasaki, S. Horiuchi, and N. Yoshida, Phys. Rev. D **90**, 063502 (2014).
[146] N. Fornengo and M. Regis, Front. Phys. **2**, 6 (2014).
[147] S. Ando, A. Benoit-Lévy, and E. Komatsu, Phys. Rev. D **90**, 023514 (2014).
[148] S. S. Campbell and J. F. Beacom, arXiv:1312.3945.
[149] S. Camera, M. Fornasa, N. Fornengo, and M. Regis, Astrophys. J. **771**, L5 (2013).
[150] D. Hooper, C. Kelso, and F. S. Queiroz, Astropart. Phys. **46**, 55 (2013).
[151] R. M. Crocker, N. F. Bell, C. Balazs, and D. I. Jones, Phys. Rev. D **81**, 063516 (2010).
[152] N. Fornengo, R. A. Lineros, M. Regis, and M. Taoso, J. Cosmol. Astropart. Phys. 01 (2012) 005.
[153] M. Wechakama and Y. Ascasibar, Mon. Not. R. Astron. Soc. **439**, 566 (2014).
[154] E. Storm, T. E. Jeltema, S. Profumo, and L. Rudnick, Astrophys. J. **768**, 106 (2013).
[155] K. Spekkens, B. S. Mason, J. E. Aguirre, and B. Nhan, Astrophys. J. **773**, 61 (2013).
[156] A. Natarajan, J. B. Peterson, T. C. Voytek, K. Spekkens, B. Mason, J. Aguirre, and B. Willman, Phys. Rev. D **88**, 083535 (2013).
[157] A. E. Egorov and E. Pierpaoli, Phys. Rev. D **88**, 023504 (2013).
[158] K. Abe *et al.*, Phys. Lett. B **670**, 103 (2008).
[159] I. G. Usoskin, G. A. Bazilevskaya, and G. A. Kovaltsov, J. Geophys. Res. **116**, A02104 (2011).
[160] L. Maccione, Phys. Rev. Lett. **110**, 081101 (2013).
[161] R. A. Caballero-Lopez and H. Moraal, J. Geophys. Res. **109**, A01101 (2004).
[162] M. Potgieter, Living Rev. Solar Phys. **10**, 3 (2013).
[163] I. Cholis, D. Hooper, and T. Linden, arXiv:1408.6224.
[164] A. Bottino, F. Donato, N. Fornengo, and P. Salati, Phys. Rev. D **58**, 123503 (1998).
[165] A. Bottino, F. Donato, N. Fornengo, and P. Salati, Phys. Rev. D **72**, 083518 (2005).
[166] J. Lavalle, Phys. Rev. D **82**, 081302 (2010).
[167] W. Detmold, M. McCullough, and A. Pochinsky, arXiv: 1406.2276.
[168] E. Jones *et al.*, "SciPy: Open source scientific tools for Python," 2001.
[169] F. James and M. Roos, Comput. Phys. Commun. **10**, 343 (1975).
[170] J. D. Hunter, Comput. Sci. Eng. **9**, 90 (2007).
[171] M. Cirelli, D. Gaggero, G. Giesen, M. Taoso, and A. Urbano, arXiv:1407.2173.